Master Thesis
TVVR 22/5010

Combining Continuous and Event-based Hydrological Modeling in Kävlinge River Basin with HEC-HMS

Hydrological Response to Climate Change and Flood Frequency Analysis

Wenli Hu

Division of Water Resources Engineering
Department of Building and Environmental Technology
Lund University

Combining Continuous and Event-based Hydrological Modelling in Kävlinge River Basin with HEC-HMS

Hydrological Response to Climate Change and Flood Frequency Analysis

By:
Wenli Hu

Master Thesis

Division of Water Resources Engineering
Department of Building & Environmental Technology
Lund University
Box 118
221 00 Lund, Sweden

Water Resources Engineering
TVVR-22/5010
ISSN 1101-9824

Lund 2022
www.tvrl.lth.s

Master Thesis
Division of Water Resources Engineering
Department of Building & Environmental Technology
Lund University

Swedish title:	Kombinera kontinuerlig och händelsebaserad hydrologisk Modellering i Kävlingeås avrinningsområde med HEC-HMS–Hydrologiska respons mot klimatförändringar och frekvensanalys för översvämningar
English title:	Combining Continuous and Event-based Hydrological Modelling in Kävlinge River Basin with HEC-HMS– Hydrological Response to Climate Change and Flood Frequency Analysis

Author:	Wenli Hu
Supervisor:	Linus Zhang
Examiner:	Erik Nilsson
Language	English
Year:	2022
Keywords:	HEC-HMS, SCS-CN, Climate Change, GIS, Flood

Acknowledgements

I would first like to thank Lund University for giving me the opportunity to study and expand my knowledge. It has been an amazing experience learning from the teaching faculty of the Department of Water Resource Engineering and Department of Engineering Geology.

I would also like to express my gratitude to Linus Zhang and Erik Nilsson for the opportunity to write the degree project at the Department of Water Resource Engineering. I have been able to profit from Linus and Erik's knowledge and experience in many insightful discussions, for which I am very grateful.

Additionally, thanks to Sebastian Huynh, Victoria Truong, and Omar Alejandro Callanaupa Tocto for acting as opponents for my thesis defending and my friend Simon Kreipl for proofreading this report.

Abstract:

Prediction of flood and evaluation of the impact of climate change in a catchment needs to be correctly estimated, which can be accomplished by hydrological modelling in HEC-HMS. In this paper, the objectives were to gain an understanding of the rainfall-runoff process and estimate the flood frequency curve in the Kävlinge River Basin. However, due to the complexity of a catchment, models should be well-calibrated and validated in order to increase predictive ability. The flood frequency estimation through simulation can be addressed through continuous or event-based hydrological modelling. Firstly, because of the data availability for short-term storms and initial soil moisture conditions, continuous models are calibrated and validated in different years. Afterwards, the identical parameters can be used for the event-based simulation. The hypothetical storm method was used to construct flood frequency curves of different return periods. Finally, all the above simulations were carried out with climate change scenario RCP8.5.

The result shows that the Curve Number (CN), initial abstraction (Ia) and Lag time are the crucial parameters for the rainfall-runoff modelling. The statistical analysis of Coefficient of Determination (R^2), Percent Bias (PBIAS) and model Peak error (%) efficiency criteria were used for performance evaluation at three stations (Högsmölla, Ellinge and Vombsjön). Most of the statistics are within an acceptable range (±30%) except the values at Vombsjön due to the regulated flow, which indicates the good performance of the hydrological modelling. As well as this, the hydrological model with RCP8.5 climate change scenario is used to evaluate the effects of climate change on continuous and flood events simulation. There are around 24% and 20% increases in peak flow respectively compared with the current condition.

Table of Contents

List of Tables

List of Figures

List of Abbreviations

SCS-CN	Soil Conservation Service Curve Number
CN	Curve Number
AMC	Antecedent Moisture Conditions
Ia	The initial abstraction
S	Potential amount storage
Pe	Accumulated precipitation excess
LT	Lag time
DEM	Digital Elevation Models
ET	Evapotranspiration
GIS	Geographic information system
LU	Land Use
LC	Land Cover
Tc	Time of concentration
Hr	Hours
Mins	Minutes

1. Introduction

1.1 General Background

Flood is one of the most frequent and devastating natural disasters, which may pose threat to life and cause economic losses and environmental destruction in many parts of the world. Therefore, it is crucial to find out the reasons and the key factors that can mitigate the damage. Floods can happen not only in big rivers but also in streams and small catchments (Maskey and ProQuest, 2004).

Floods can be characterized in serval types, such as urban floods, coastal floods, river floods, and flash floods. In this case study, only flash floods and river floods will be modelled and analyzed. Further, the analysis will be carried out with climate change scenarios. The predicted increase in precipitation and temperature would be more frequent and intense than before. The assumption is based on the two-degree overall increase in temperature expected by 2100. Rainier summers, as well as earlier snow melting, are expected to occur due to climate change in Skåne. Also, precipitation in Sweden is expected to rise. By the end of the century, the average annual precipitation will be 16% more than for the period 1961-1990 with climate change scenario RCP8.5. The same rainstorm event from 1961 to 1990 that occurred once every 20 years will occur as a 4 to 8-year return period storm at the end of the century based on the Climate Secure Sweden report (Hall et al., 2015).

In the present paper, meteorological conditions and initial catchment wetness have a significant impact on cumulative outflow and peak discharge (Czigány, Pirkhoffer and Geresdi, 2010). For the meteorological condition, there is a non-linear relationship between the precipitation and runoff generation both in continuous and event-based simulation, which brings uncertainties to the hydrological modelling(Bahramian *et al.*, 2021). Regarding initial catchment wetness, it has a material impact on the peak and volume of a flood event (Chifflard *et al.*, 2018). Also, soil moisture varies significantly in both space and time and it is difficult to measure, the variation range can be estimated by applying some empirical formula. Hence, the extent to corresponding soil moisture that buffers the extreme precipitation could also be estimated with different simulations.

Modelling techniques have become more important as they help visualize the current flood risks and estimate the further risks as well. Hydrologic modelling can be used to estimate instantaneous streamflow over river basins and compare the simulated stream and observed flow for predicting the hydrologic process. There are a couple of models, such as MIKE-SHE, SWAT, and TOPMODEL, and these demand a considerable amount of data. HEC-HMS (The Hydrologic Modeling System) is another open-source software that can be easily accessed and has extensive applications.

In this case study, an attempt is made to understand the hydrology of the Kävlinge River Catchment. In order to understand the extreme rainfall-runoff mechanism, a digital elevation map, land cover distribution, soil type variations, and historic data regarding precipitation (for producing the precipitation return period) are put into use in a hydrologic model.

1.2 Objectives and Research Questions

The aim of this investigation is to develop a physically-based hydrological model with HEC-HMS and simulate the effects of extreme rainfall on surface runoff and discharges. In addition, the study also aims to evaluate the performance of the models by doing a thorough frequency analysis.

The following research questions are specifically highlighted by the mentioned objectives:

- How to Calibrate and validate the direct runoff and peak discharges in the catchment both in continuous and event-based simulation and analyze how the possible processes and parameters (ie. soil moisture) influence the result?
- How to assess the impacts of climate change on the hydrological model?
- How to estimate the flood and analyze flood frequency?

To investigate the potential answers to the above questions, a HEC-HMS hydrological model will be developed for the Kävlinge River Basin. The significance of different model parameters will be analyzed and discussed by conducting a thorough sensitivity check.

1.3 Study Area

The geographic location of the Kävlinge River Basin is situated in the southernmost province of Skåne in Sweden stretching from the east Baltic sea to the Öresund sea in the west, as seen in Figure 1. It covers an area of around 1204 km2 that includes the large lakes Vombsjön, Krankesjön, Ellestadssjön, Snogeholmssjön, and Sövdesjön. The major tributaries are Bråån in the north, Klingavälsån in the south, and Björkaån in the east(Vattenrådet – Kävlingeån, 2022).

There are three observation stations, Högsmölla (close to the outlet), Ellinge (in the northwest), and Vombsjön (in the central part).

67,000 inhabitants live in the catchment area and 75% of them live in the area's urban areas. Eslöv, Kävlinge, Sjöbo are the lager ones (Vattenrådet – Kävlingeån, 2022).

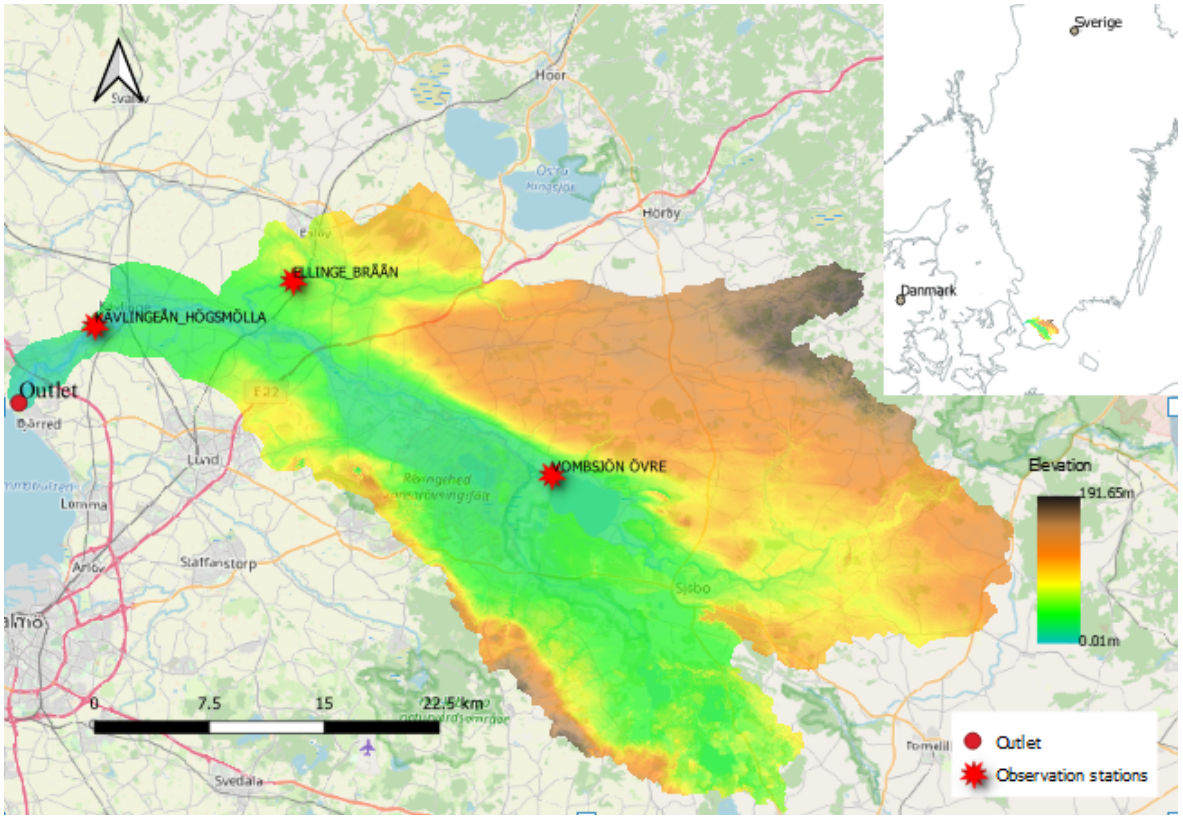

Figure 1: Map of the Study Area

2. Climate Change

The Swedish Meteorological and Hydrological Institute provides the service of observations and scenarios from different regional climate models by several different global climate models. The climate models are provided with a High-resolution 12.5 ×12.5 km, which enables them to show more detailed results. The measure of radiation power (W/m^2) is used to evaluate how the greenhouse effect will change in the future, the more greenhouse gas emissions, the more radiation power. Several scenarios are provided, and RCP8.5 climate change model data is used in the Kävlinge River Basin since it leads to the most extreme conditions. The RCP8.5 climate change scenario indicates that the solar radiation is going to increase to 8.5W/m² and comparatively high greenhouse gas emissions.

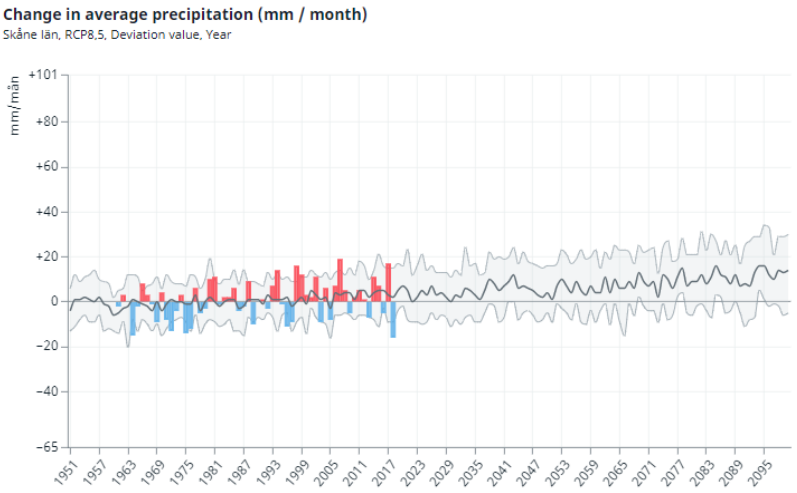

Figure 2: Estimated change in average precipitation (mm) for the period 2071–2100 compared with 1971 - 2000. The graph is based on an average of an ensemble of a number of climate scenarios for scenario RCP8.5 (SMHI,2022).

Figure 2 illustrates the yearly precipitation percent variation from 2000 to 2100 compared with the reference time period between 1961 and 1990 in Skåne. The ascending red bars show the precipitation higher than normal and the descending blue bars show precipitation lower than normal. The grey curve represents the average of several climate models for scenario RCP8.5 and the grey area indicates the range from 10^{th} and 90^{th} percentiles.

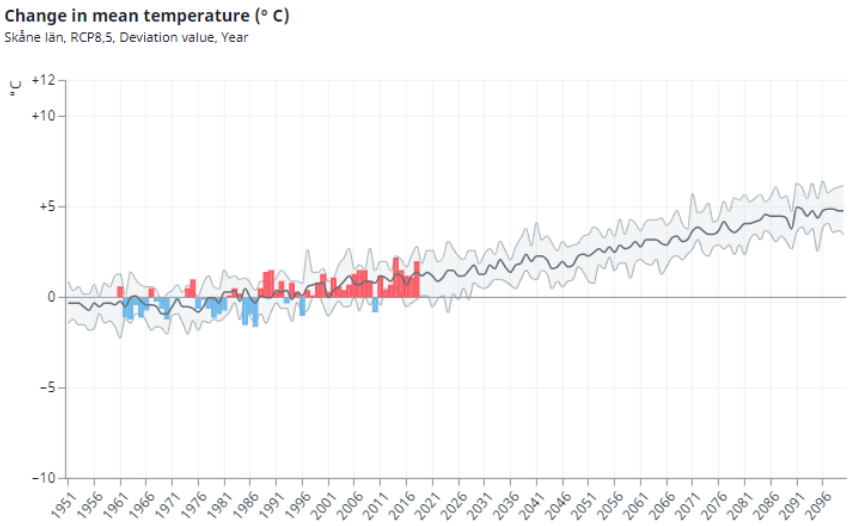

Figure 3: Estimated change in average temperature (° C) for the period 2071–2100 in comparison to 1971 - 2000. The graph is based on an average of an ensemble of a number of climate scenarios for scenario RCP8.5 (SMHI, 2022)

The changes in average temperature (° C) in Skåne County during the time 1951–2100 in contrast to the normal (average value for 1971–2000) is shown in Figure 3. Also, based on the historical data, the ascending red bars illustrate temperatures greater than normal and descending blue bars temperatures less than normal. The grey curve shows an average of several climate models for scenario RCP8.5. The grey region illustrates the range of variation between the 10th and 90th percentiles (SMHI,2022).

Table 1: Increase in Yearly Precipitation in Skåne: Average climate model predicted a percent increase from average values during the period 1961-1990 (SMHI, 2022).

Year	2091	2092	2093	2094	**2095**	2096	2097	2098	2099	2100
%	8	7	13	16	**16**	12	10	14	13	14

As was discussed before, generally, there is an increasing trend in precipitation with time. The time close to 2100 will be chosen as a comparison since it results in the most severe scenario. Table 1 shows that the year 2095 will produce the heaviest precipitation. The reference period is from October 2019 to March 2020. This time period was chosen because they are the most recent year also the Vombjösn Lake has had a minimum impact during these seasons (the heavy precipitation does not produce higher water flow due to the Vombjösn Lake buffering during the rainy season). The percentage of 16% for the year 2095 was used to modify available precipitation gauge data to a dataset for a climate change model. The reference period (half a year) has a total precipitation average of 332.33 mm. The year 2095 with a 16 percent increase is expected to have a corresponding precipitation average of 385.51 mm.

Table 2: Increase in yearly temperature in Skåne: Average climate model predicted percent increase from average values from the period 1961-1990 (SMHI, 2022).

Year	2091	2092	2093	2094	2095	2096	2097	2098	2099	2100
%	5	4.9	4.5	4.8	**4.4**	4.8	4.9	4.9	4.8	4.8

HEC-HMS snowmelt simulation requires temperature data for each timestep. They are used to determine whether precipitation falls as rain or snow as an index for all of the energy fluxes into the snowpack. Therefore, it also has a great impact on runoff generation. The year 2095 will be chosen accordingly with an increasing percentage of 4.4%. The data will be modified from the temperature gauge for a Climate change model.

3. HEC-HMS Model and Data Collection

HEC-HMS are selected to simulate the rainfall-runoff processes of dendritic watershed systems. It can be applied for modelling the large river basin and small urban or natural watershed runoff. A wide range of methods is available to estimate runoff from catchments, using observed data or empirical and statistical techniques to estimate river discharge. These are commonly known as rainfall-runoff models (Scharffenberg, 2013). HEC-HMS river basin modelling has been developed by the Hydrologic Engineering Center with the American Army Corps of Engineers since 1989.

All Rainfall-Runoff models are the simplified characterizations of the real-world system (Moradkhani and Sorooshian, 2008). While they help to visualise the response in the catchment because of variations in land use, soil types, meteorological events, etc. The hierarchical structure of the model is created with three components, basin models, meteorologic models, and control specifications. The build-in GIS-based physical basin model tool for HEC-HMS was used to delineate the river basin, extracting watershed physical characteristics from DEM (Digital Elevation Model).

The meteorological model is used to simulate precipitation within the basin. Information regarding meteorological components such as temperature, precipitation evapotranspiration, sunshine, humidity, and snowmelt is defined in the meteorological model. HEC-HMS provides a variety of options to define each meteorological element. The latest HEC-HMS 4.10 version was used during this project. Tutorials can be found on the following website (https://www.hec.usace.army.mil/software/hec-hms/).

Different components included in the HEC-HMS are as follows:

- Basin Models, methods and parameters: the following hydrologic elements (subbasins, junctions, reaches, reservoirs) and drainage network of the physical basin area are involved in basin models.

  Parameters of loss method: Initial abstraction (mm) and Curve number.

  Parameters of transform method: Lag time (mins) and peak rate factor.

Parameters of base flow method: Recession constant and ratio to the peak.

Parameters of reach routing: Muskingum K (hr) and Muskingum X.

- Meteorological Models: All files in the meteorological model are stored and managed using the HEC-DSS format or manual input data, including temperature, precipitation evapotranspiration, sunshine, and humidity. Evaporation and snowmelt are defined in the meteorological model. A bunch of methods are provided to define each meteorological element.

- Control Specification: Starting date and time, ending date and time and computational time step for the simulation are defined in this component.

- Time Series Data: Real-time series data (precipitation, temperature data) for all the meteorological elements defined in the meteorological model are fed in this part. Apart from the above-mentioned meteorological element, discharge data can also be supplied for calibration and simulation of the developed model. It can be input manually or in the form of HEC-DSS in the Hydrologic Engineering Center Data Storage System.

3.1 Data Collection

3.1.1 Digital Elevation Model

The topographic feature of the study area is presented as DEM (Digital Elevation Model).DEM tiles of resolution of approximately 2 m for the basin were downloaded from the Swedish National Land Survey's Geoportal (Lantmäteriet, 2022), and then merged and projected to SWEREF99 TM to one tile. This DEM was clipped within the watershed using the polygon shapefile of the catchment from the above website as well (Figure 4).

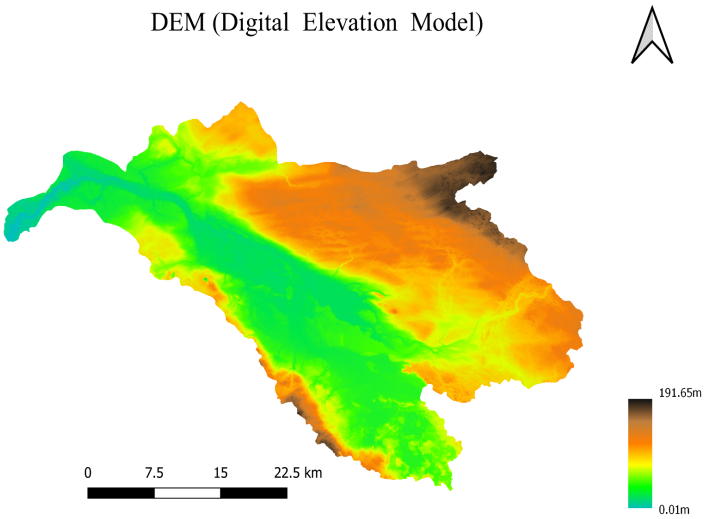

Figure 4: Projected DEM of the catchment

3.1.2 Land Cover Map

The land cover map including imperviousness area was derived from the land cover files downloaded from the Environment Rating Scales Institute (ERSI, 2022). The map was downloaded and classified based on the Food and Agriculture Organization of the United Nations. In order to facilitate the Curve number calculation, the land cover map is reclassified into the water, urban area, forest, and agriculture area (in Figure 5) in QGIS. The unsupervised classification method was used in this study. After the classification, every class needs to be inspected and assigned a name.

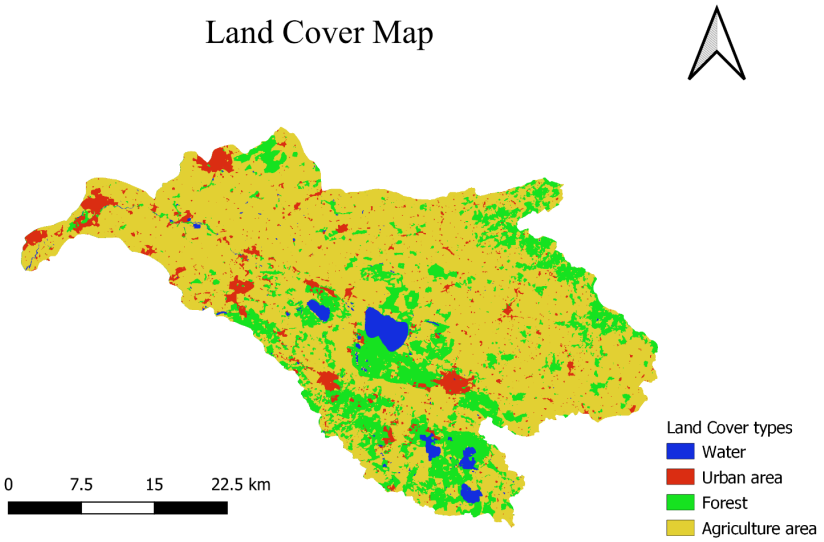

Figure 5: Land cover map of Kävlinge river basin

Table 3: Areal Distribution of different Land use

No.	Land use	Area (km^2)	Percentage (%)
1	Water	28.30	2.35
2	Urban area	69.02	5.74
3	Forest	243.22	20.22
4	Agriculture area	862.30	71.69
5	Total	1202.83	100

3.1.3 Soil Map

Global Hydrologic Soil Groups (HYSOGs250m) for Curve Number-Based Runoff Modeling was downloaded from Earth Data (ROSS *et al.*, 2018), which can be put into use directly for creating

Curve Number. The Global Hydrologic Soil Groups is built up for generating Curve numbers. The data type is Raster data with a resolution of 250m, which represents the rainfall-runoff potential (Figure 6). There are four categories: **A)** Sand or water **B)** Sandy loam, Loamy sand **C)** Clay loam, Silty clay loam, sandy clay loam, Loam, Silty loam, Silt **D)** Clay, Silty clay, Sandy clay. The four classes A, B, C, and D correspond to soils with low, moderately low, moderately high, and high runoff potential, respectively in Table 4.

Table 4: Soil textures classification (USDA,1986)

Group	Minimum Infiltration Rate (mm/hr)	Soil type
A	>7.62	High infiltration rates, deep, well-drained sand and gravels
B	3.81-7.62	Moderate infiltration rates, moderately deep, moderately well-drained soils with moderately coarse textures
C	1.27-3.81	slow infiltration rates, soils with layers, or soils with moderately fine textures
D	0-1.27	Very low infiltration rates, clayey soils high water table, or shallow impervious layer

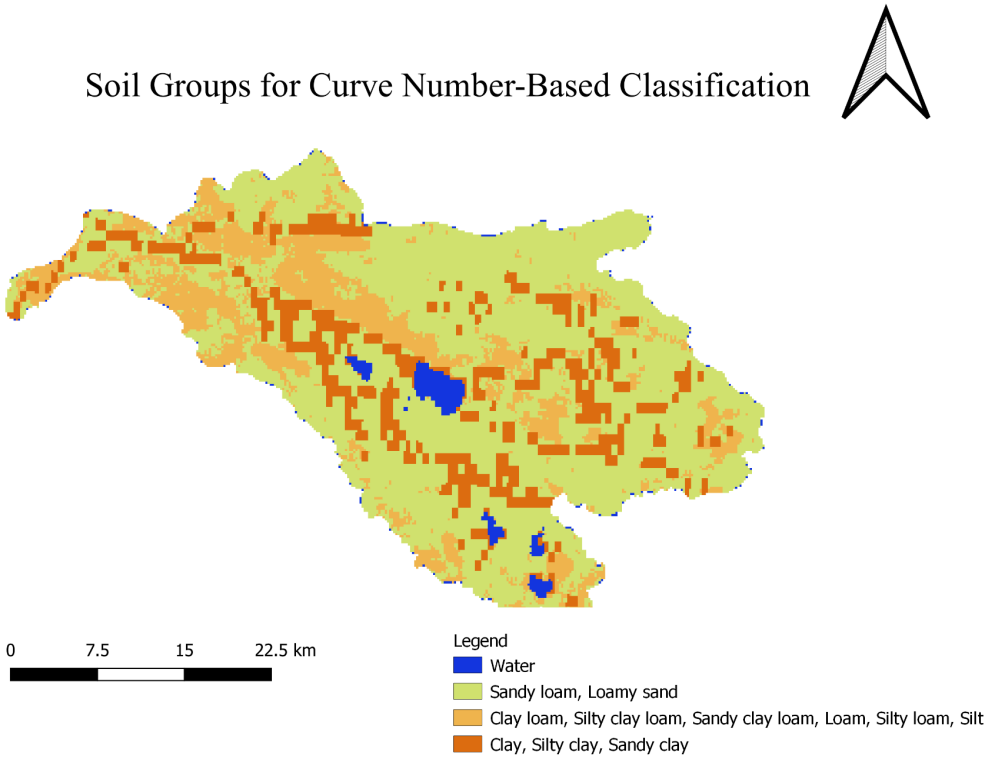

Figure 6: Soil *map of Kävlinge river basin*

3.1.4 Curve Number (CN) Map

In the HEC HMS model, the Curve Number (CN) is a simplified factor influenced by soil properties, geological formation and land use. The value of the CN (curve number) varies between 100 (for waterlogged surfaces) and 30 (for non-watertight surfaces). The curve number (CN) grid was created in Q-GIS using land use and soil type layers (Figure 7). Then, the CN values for each subbasin were optimized during calibration. It depends both on the land use difference and the soil conditions. In order to get the SCS curve number, the combination of land use and soil groups should be conducted in Table 5. For the land use, it is reclassified into 4 classes (water, urban area, forest, and Agriculture area) based on the original land use classification. Also, soil groups (4 classes) are classified by different minimum infiltration rates in Table 4.

Table 5: Combination of Land use and Soil group for generating Curve number

Land use	Value	Soil Hydrologic Group			
		A (1)	B (2)	C (3)	D (4)
Water	1	100	100	100	100
Urban area	2	54	70	80	85
Forest	3	32	58	72	79
Agricultural area	4	67	78	85	89

The following steps are applied in order to obtain CN grid map:

- Landuse.tif (Landuse raster)
- Soil groups.tif (Soil groups raster)
- Boundary.shp (shapefile with watershed boundary)
- Class table.txt (Landuse classification table in a comma-separated file)
- Component.txt (Component table with soil properties in a comma-separated file)
- CN-query.txt (Raster query expression in a text file)
- Zonal statistics (Combine the subbasins shapefile generated from Terrain data processing with CN grid map)

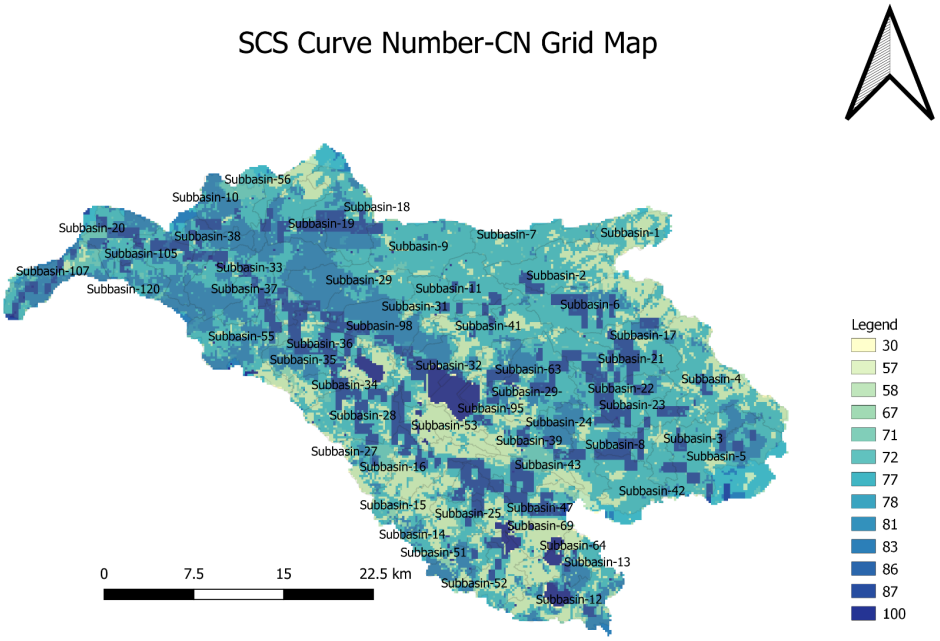

Figure 7: CN grid map of Kävlinge river basin

Estimating CN for each subbasin:

After generating the CN values, the values are assigned to each subbasin by using zonal statistics in Q-GIS. Further, the time of concentration (T_c), lag time (T_{lag}), potential maximum retention (S), and the initial abstraction (I_a) will be also calculated by using the following empirical methods. The detailed theory will be discussed in chapter 3.2.

$$Tc = (L)^{0.8} * (1000/CN - 9)^{0.7}/441Y^{0.5} \quad (1)$$

Tc= time of concentration, L= length of the mainstream to farthest divide, Y = average watershed slope %, CN= Curve Number.

$$T_{lag} = 0.6 * T_c \quad (2)$$

T_{lag} = lag time.

$$S = (25400 - 254CN)/CN \quad (3)$$

S = The maximum retention (mm)

$$I_a = 0.2S \quad (4)$$

I_a = Initial abstraction

Table 6: Initial values of different parameters for each sub-basin

No.	CN value	Time of concentration (mins)	lag time (mins)	Maximum retention-S (mm)	Initial abstraction (0.2S)
Subbasin-1	68.99	306.88	184.13	11.41	2.28
Subbasin-10	79.24	285.85	171.51	66.53	13.31
Subbasin-101	81.40	171.66	103.00	58.04	11.61
Subbasin-105	81.46	335.31	201.19	57.80	11.56
Subbasin-107	79.63	433.66	260.19	64.97	12.99
Subbasin-11	76.83	281.44	168.86	76.60	15.32
Subbasin-12	76.21	232.57	139.54	79.30	15.86
Subbasin-120	80.23	379.89	227.94	62.59	12.52
Subbasin-13	71.72	197.40	118.44	100.16	20.03
Subbasin-14	71.44	281.65	168.99	101.54	20.31
Subbasin-15	68.91	307.04	184.23	114.57	22.91
Subbasin-16	68.42	328.45	197.07	117.24	23.45
Subbasin-17	75.33	268.11	160.87	83.20	16.64
Subbasin-18	79.24	327.86	196.71	66.53	13.31
Subbasin-19	78.29	316.58	189.95	70.44	14.09
Subbasin-2	73.11	426.69	256.02	93.44	18.69
Subbasin-20	80.45	259.37	155.62	61.73	12.35
Subbasin-21	79.79	243.63	146.18	64.35	12.87
Subbasin-22	79.72	307.00	184.20	64.61	12.92
Subbasin-23	79.20	203.79	122.27	66.69	13.34
Subbasin-24	79.13	263.01	157.81	66.99	13.40
Subbasin-25	72.46	319.21	191.52	96.53	19.31
Subbasin-26	75.53	201.47	120.88	82.28	16.46
Subbasin-27	72.80	249.53	149.72	94.88	18.98
Subbasin-28	75.39	396.34	237.80	82.90	16.58
Subbasin-29	81.69	314.95	188.97	56.94	11.39
Subbasin-3	76.93	368.29	220.97	76.17	15.23

Subbasin-30	77.11	171.41	102.85	75.42	15.08
Subbasin-31	76.73	344.28	206.57	77.02	15.40
Subbasin-32	81.05	243.75	146.25	59.37	11.87
Subbasin-33	80.74	380.03	228.02	60.61	12.12
Subbasin-34	73.16	265.57	159.34	93.20	18.64
Subbasin-35	80.42	206.92	124.15	61.83	12.37
Subbasin-36	78.49	379.90	227.94	69.62	13.92
Subbasin-37	80.98	246.80	148.08	59.67	11.93
Subbasin-38	82.27	248.49	149.09	54.74	10.95
Subbasin-39	73.41	476.63	285.98	91.99	18.40
Subbasin-4	71.81	392.02	235.21	99.73	19.95
Subbasin-41	72.61	468.15	280.89	95.80	19.16
Subbasin-42	75.76	311.49	186.90	81.28	16.26
Subbasin-43	76.87	309.78	185.87	76.42	15.28
Subbasin-47	76.11	373.37	224.02	79.72	15.94
Subbasin-5	78.68	327.99	196.79	68.81	13.76
Subbasin-51	76.69	254.29	152.57	77.21	15.44
Subbasin-52	71.46	250.05	150.03	101.43	20.29
Subbasin-53	64.29	646.04	387.62	141.09	28.22
Subbasin-55	77.42	414.99	248.99	74.08	14.82
Subbasin-56	69.22	408.20	244.92	112.92	22.58
Subbasin-6	75.54	341.59	204.95	82.26	16.45
Subbasin-63	75.57	266.44	159.87	82.13	16.43
Subbasin-64	68.53	262.85	157.71	116.66	23.33
Subbasin-69	79.00	55.38	33.23	67.52	13.50
Subbasin-7	75.40	490.19	294.12	82.86	16.57
Subbasin-76	81.76	277.50	166.50	56.66	11.33
Subbasin-8	77.46	128.99	77.39	73.93	14.79
Subbasin-81	78.42	350.09	210.05	69.88	13.98

Subbasin-9	76.68	438.71	263.23	77.23	15.45
Subbasin-90	82.32	113.04	67.83	54.54	10.91
Subbasin-92	78.75	393.17	235.90	68.55	13.71
Subbasin-95	87.98	195.94	117.56	34.70	6.94
Subbasin-98	81.82	294.32	176.59	56.42	11.28

3.1.5 Climate Data

Kävlinge catchment is located in the southernmost part of Sweden which has a temperate climate with four distinct seasons. Generally, the southern part of Sweden has a temperate oceanic climate. Precipitation takes place throughout the year and the maximum precipitation used to happen between June and September. The average precipitation varies from 664 mm to 874 mm per year. Snow can also be seen as a common form of precipitation during winter. In addition, the annual average runoff is around 8-12 l/s km². The annual average temperature is about 7.9 °C. The temperature varied between -8 ℃ in winter and 24℃ during summer on average in a year (SMHI, 2022).

The Meteorological data, such as daily precipitation (Figure 10), and temperature (Figure 11) of some stations with their respective geographical locations were downloaded from the Swedish Meteorological and Hydrological Institute (SMHI, 2022).

Also, Figure 8 shows the average monthly rainfall distribution over years at major stations (Ystad, Tomelilla, Landskrona, Lövestad, Stehag, Lund). The heaviest precipitation used to occur in August, September and October, while due to the Vombsjon Lake buffering, the peak flow used to occur between January and March (Vattenrådet – Kävlingeån, 2022).

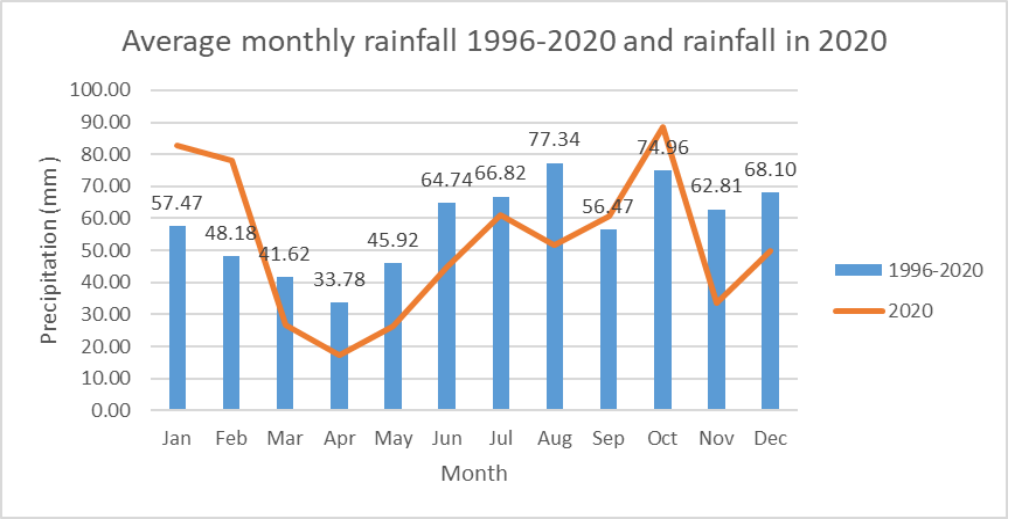

Figure 8: Monthly rainfall distribution over years and in 2020

Thiessen Polygon Method:

In order to get an accurate estimation of the spatial distribution of precipitation, it is necessary to use interpolation methods. Thiessen Polygon Method is widely used in engineering praxis, which allows the user to assign weight at each gauge station in proportion to the catchment area. However, it is also good to notice the disadvantages of this method. In mountainous areas, for instance, the spatial distribution of precipitation varies over small distances, and in such circumstances, this method may yield erroneous results. The slope in the Kävlinge river basin is less than 5% generally so the method can be applied to this catchment. The following steps are applied for constructing the polygon:

- The Gauge network is displayed on a map of the catchment area of interest.
- Adjacent stations are connected with lines.
- Perpendicular bisectors of each line are constructed (perpendicular line at the midpoint of each line connecting two stations)
- The bisectors are extended and used to form the polygon around each gauge station.
- The precipitation value for each gauge station is multiplied by the area of each polygon.
- All values from the latest step are summed and divided by the total catchment area.

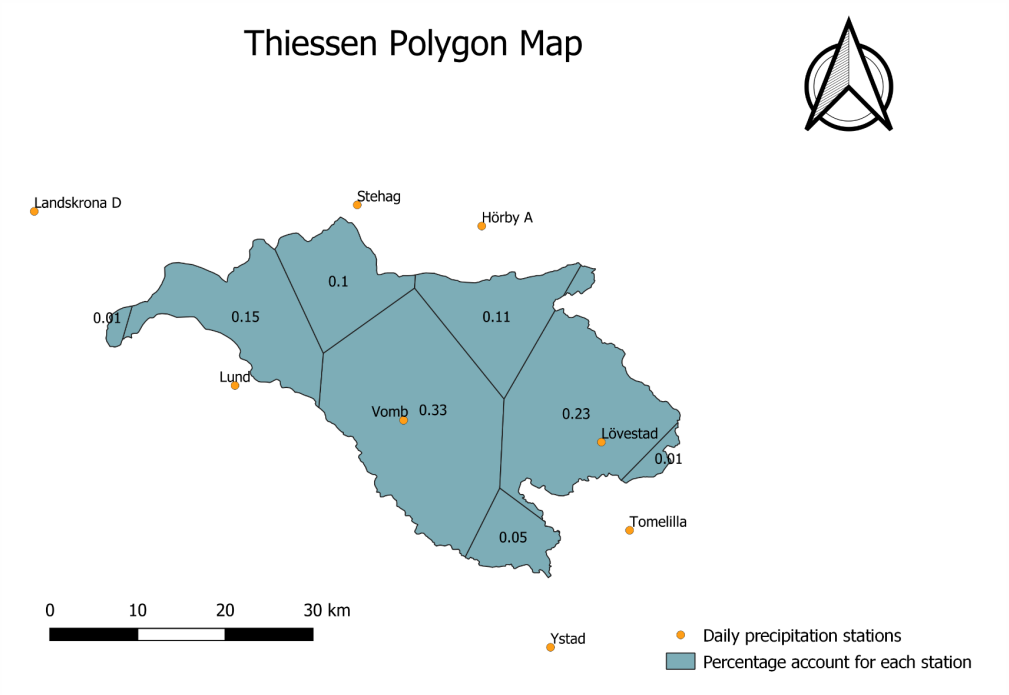

Figure 9 Thiessen Polygon Map

Checking of spatial homogeneity:

Figure 10 shows the spatial homogeneity of precipitation data for multiple series at neighbouring stations. In general, it can be observed that most of the precipitation distribution at nearby stations overlapped with each other although there are still some differences.

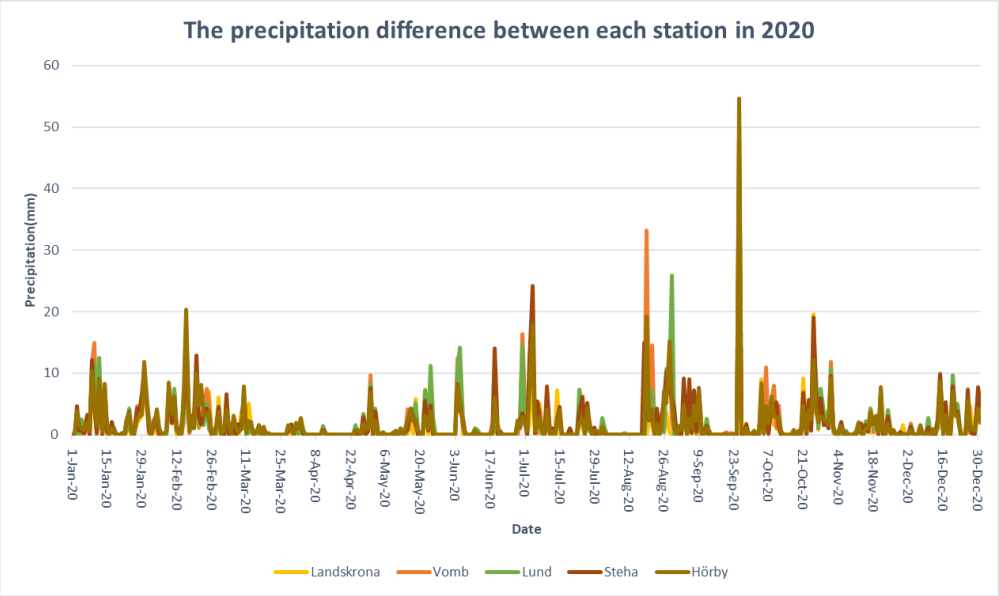

Figure 10: Precipitation distribution and the difference between each station in 2020

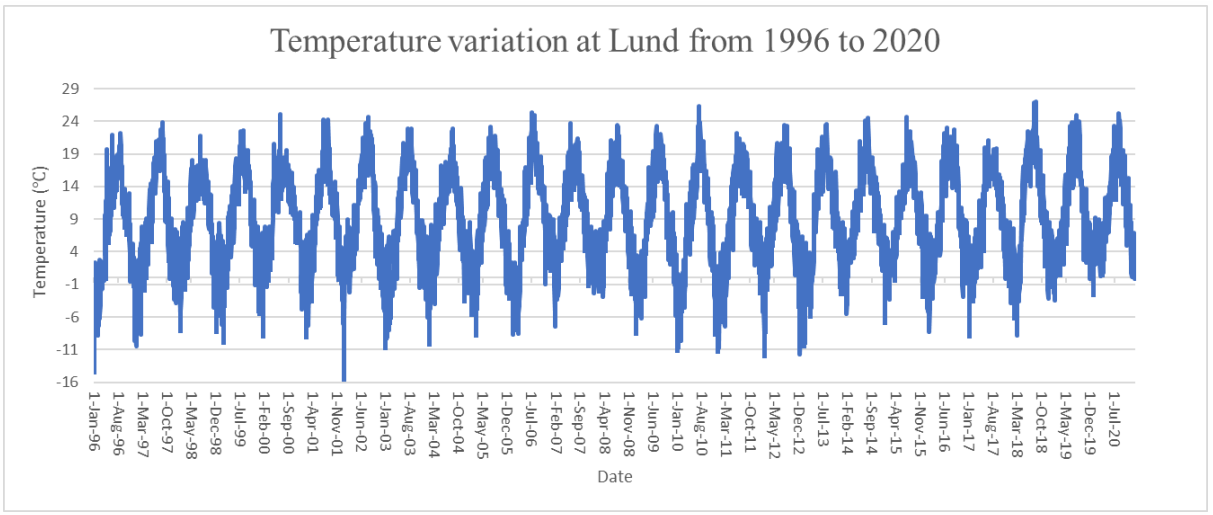

Figure 11: Temperature variation at Lund from 1996 to 2020

Also, the double mass curve method is used to evaluate the correlation between the consistency of precipitation data. The theory of the double-mass curve is based on the plot of the two cumulative quantities during the same period showing a straight line so long as the proportionality between the two remains unchanged, and the slope of the line represents the proportionality. This method can

smooth a time series and suppress random elements in the series, and thus show the main trends of the time series. The formula is used as follows:

$$Mc = c/a \times Ma \quad (5)$$

Mc =Adjusted precipitation, Ma = Observed precipitation, c = Slope of the graph to which records are adjusted, a =Slope of the graph at time Ma was observed.

Figure 12 shows a high correlation between the Cumulative annual precipitation at Lund and the Cumulative annual precipitation at adjacent four stations. There is almost no difference (R^2 = 0.99 or c/a=0.99) during the time, otherwise, the corrections should be made accordingly.

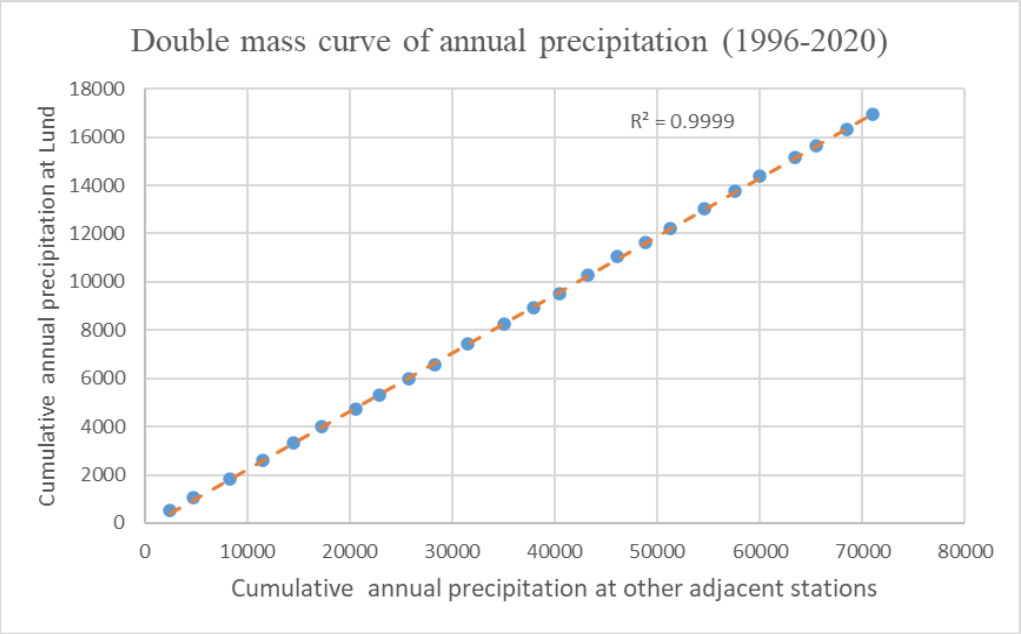

Figure 12: Double mass curve of annual precipitation 1996-2020

Frequency analysis of precipitation:

After checking the spatial homogeneity of precipitation data, Lund station (Figure 13) is used for plotting an IDF curve (intensity-duration frequency) to represent the precipitation distribution because it has a relatively longer precipitation record than other stations (more than 100 years). Then, the precipitation intensity corresponding to 24 hours duration with different return periods will be used for hypothetical storm simulation afterwards. The procedures are carried out in the following steps.

IDF curve calculation procedures:

- Daily precipitation data were collected for several years.
- Rank order: the precipitation amount and calculate return period using Weibull formula:

$$T = (n + 1)/m \quad (6)$$

T = return period (years), n = total number of years of data, m = year rank of the particular data point.

- Interpolate for return frequency of interest.
- Plot data: x-axis is the return period (years), the y-axis is intensity (mm/day)

$$P = 1/T \quad (7)$$

P = probability.

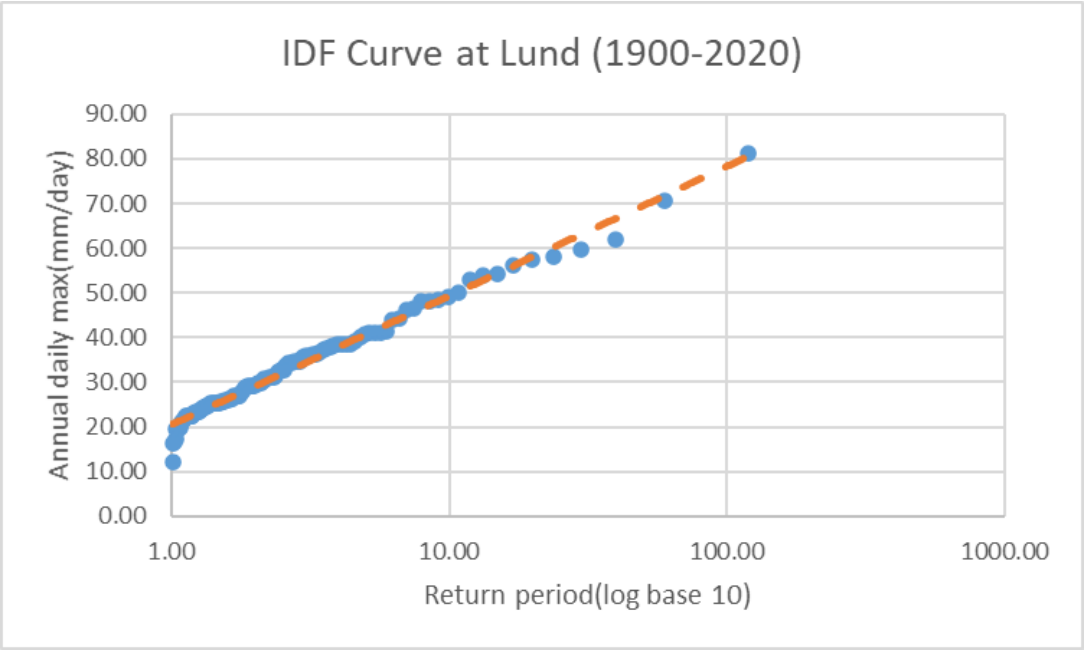

Figure 13: IDF curve based on Lund station (1900-2020)

Table 7 The average rainfall intensity with corresponding return period

Return period (Years)	2 years	5 years	10 years	25 years	50 years	100 years
Precipitation (mm)	29.35	40.76	49.09	58.5	66.38	77.82

3.1.6 Hydrology and Drainage

The Kävlinge catchment has a dendritic drainage system with rivers flowing from east to west of Sweden and entering into Öresund. The watershed area is mainly covered by arable land. It can be observed that the area along the main river, between Vombsjön and the sea, along Bråån in the north, and around Vollsjöån in the east are intensively cultivated parts. More cultivated land and forest are located in the southern part of the area, in the northern part of Romeleåsen, and around the lake landscape between Ellestadssjön and Krankesjön. The northeastern parts are dominated by forests and pastures (Vattenrådet – Kävlingeån, 2022).

The flow data were downloaded from SMHI for recent 25 years and used to calibrate the model at different stations (Table 8). Figures 14 and 15 show the discharge variation from 1996 to 2006. It can be observed that there is a decreasing trend in recent years. Also, Figures 16-18 illustrate the seasonal variation of water flow, which indicates the peak discharge usually occurs between February and March or November and December. Therefore, the calibration periods between October to the next year March were chosen for a couple of years.

Table 8: Flow Station Statistics from 1996 to 2020 (SMHI, 2022)

Item	Ellinge	Högsmölla	Vombsjön
Drainage area (km²)	150.7	1184.6	447.22
Average flow (m³/s)	1.77	10.94	3.82
Period	1996 - 2020	1996 - 2020	1996 - 2020

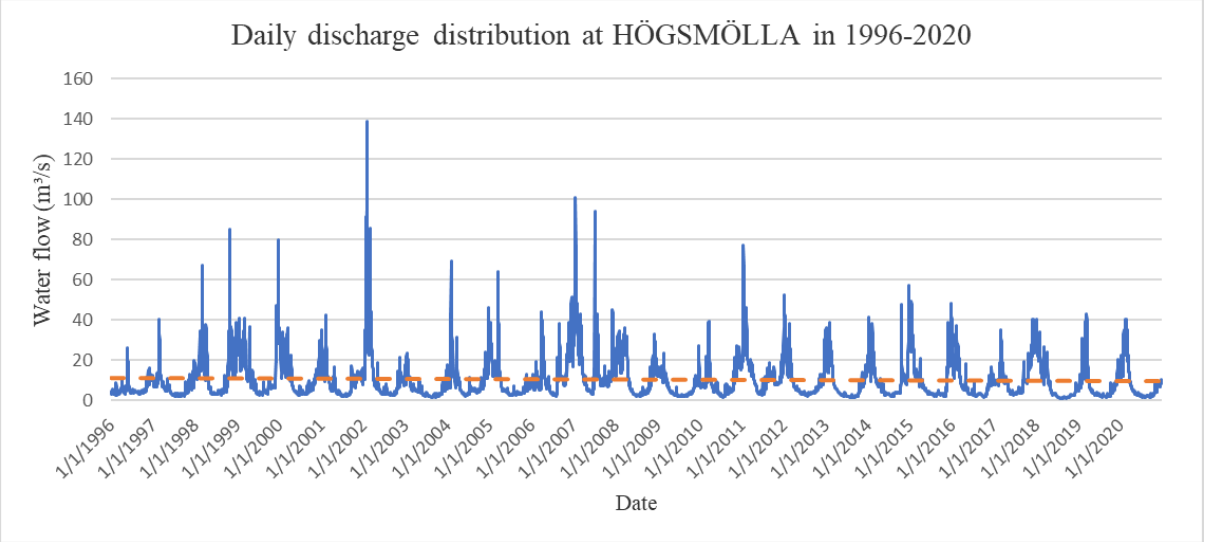

Figure 14: Hydrographs at HÖGSMÖLLA stations.

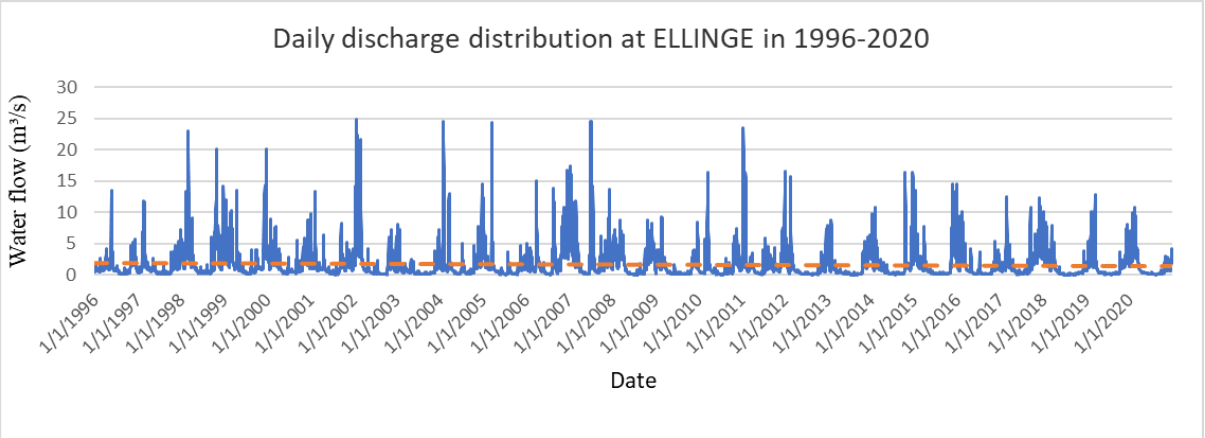

Figure 15: Hydrographs at Ellinge stations.

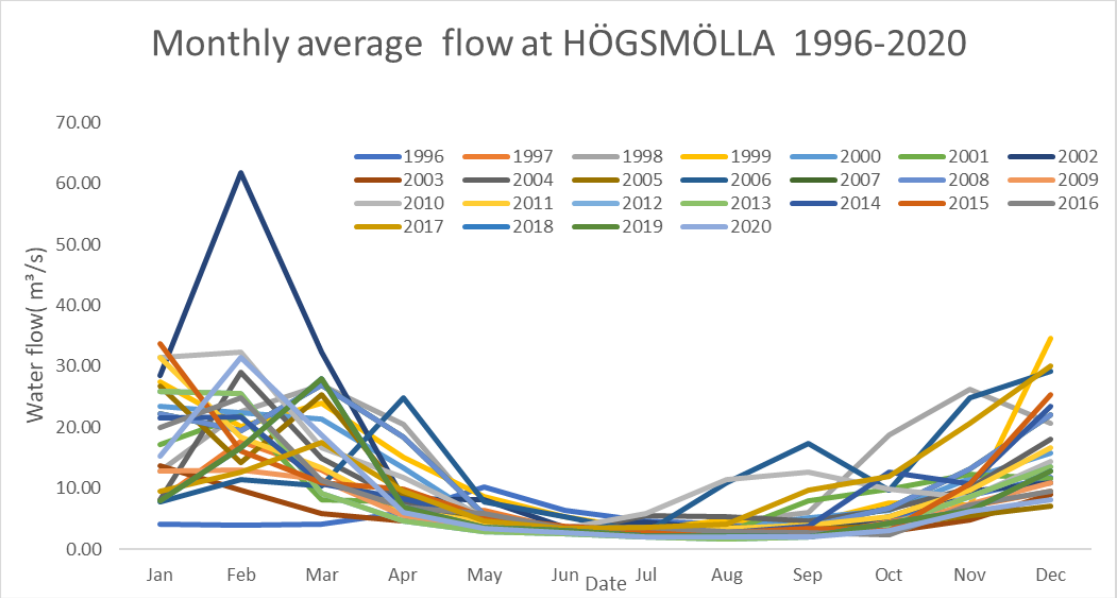

Figure 16: Monthly average flow at Högsmölla 1996-2020

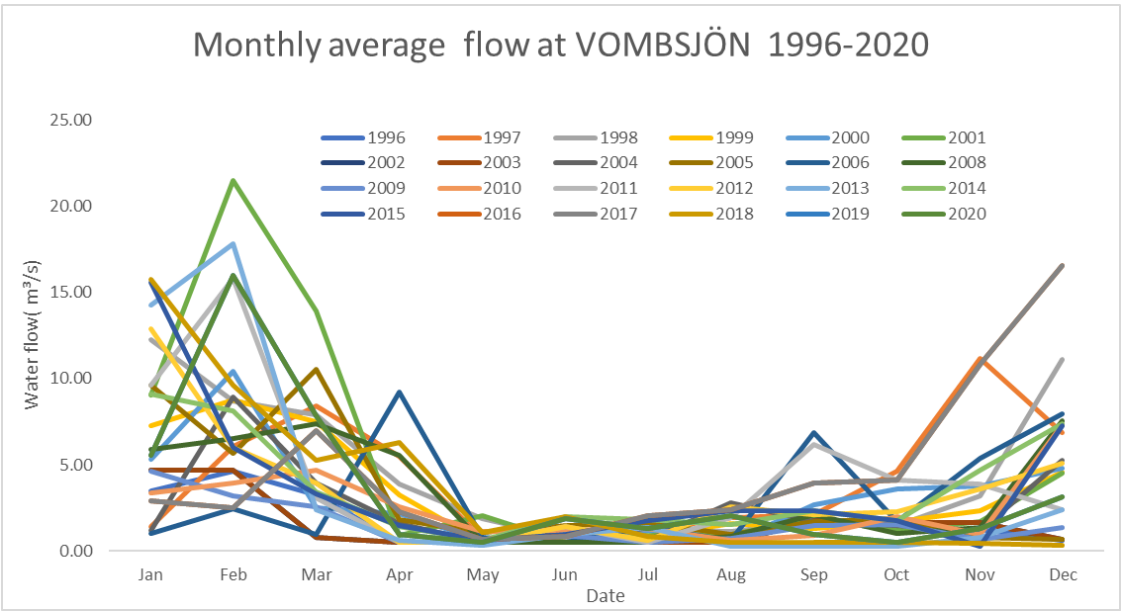

Figure 17: Monthly average flow at Vombsjön 1996-2020

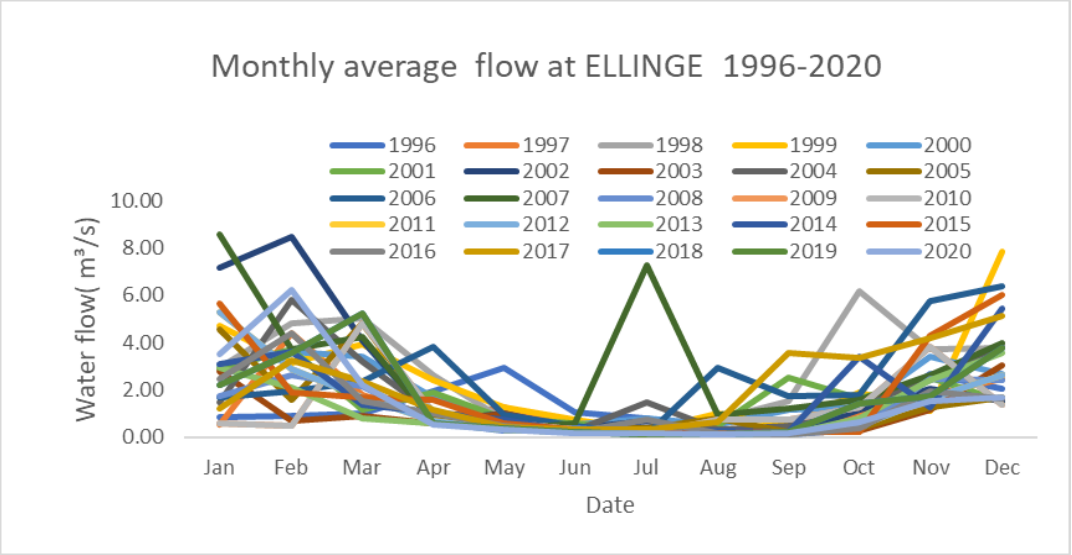

Figure 18: Monthly average flow at Ellinge 1996-2020

3.1.7 Flood Frequency Analysis

Flood frequency analysis is used to predict design floods. The reason for using the statistical method is that it can infer the parent distribution by using limited sample data. In this study, there are only 45 years of time series discharge data available. The observed annual peak flow data from 1976 to 2021 (Figure 19) is used to calculate statistical information, such as mean values, standard deviations, skewness, kurtosis, and return period. Then, the frequency distributions can be constructed by using the statistical data, which show the likelihood of different discharges as a function of recurrence interval or exceedance probability (England Jr. *et al.*, 2019).

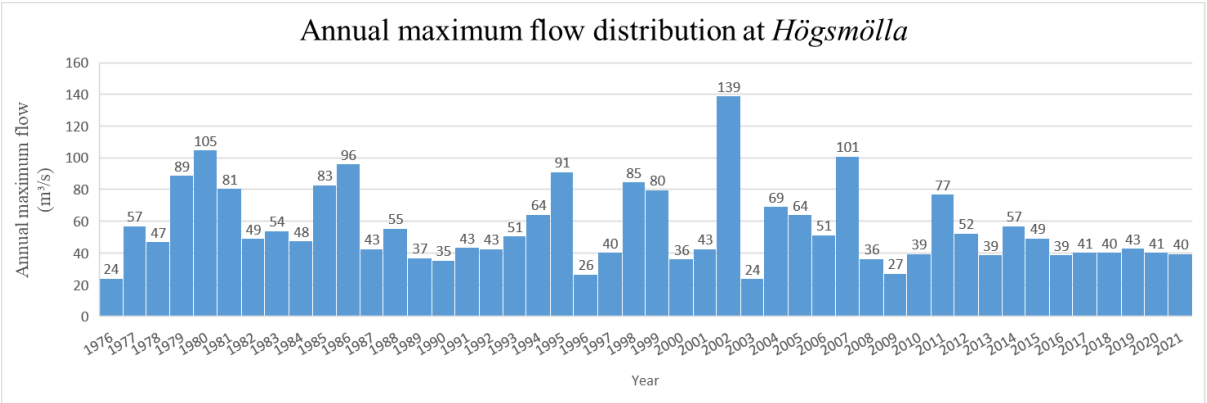

Figure 19: Annual maximum flow distribution at Högsmölla from 1976-2021

There are many forms of flood frequency distribution depending on the equations used to carry out the statistical analyses. In order to figure out which form of flood frequency distribution gives the best goodness-of-fit, HEC-SSP software is used to analyze the distribution fitness. In Figure 20, it can be observed that Log-Pearson Type III Distribution fits better than others.

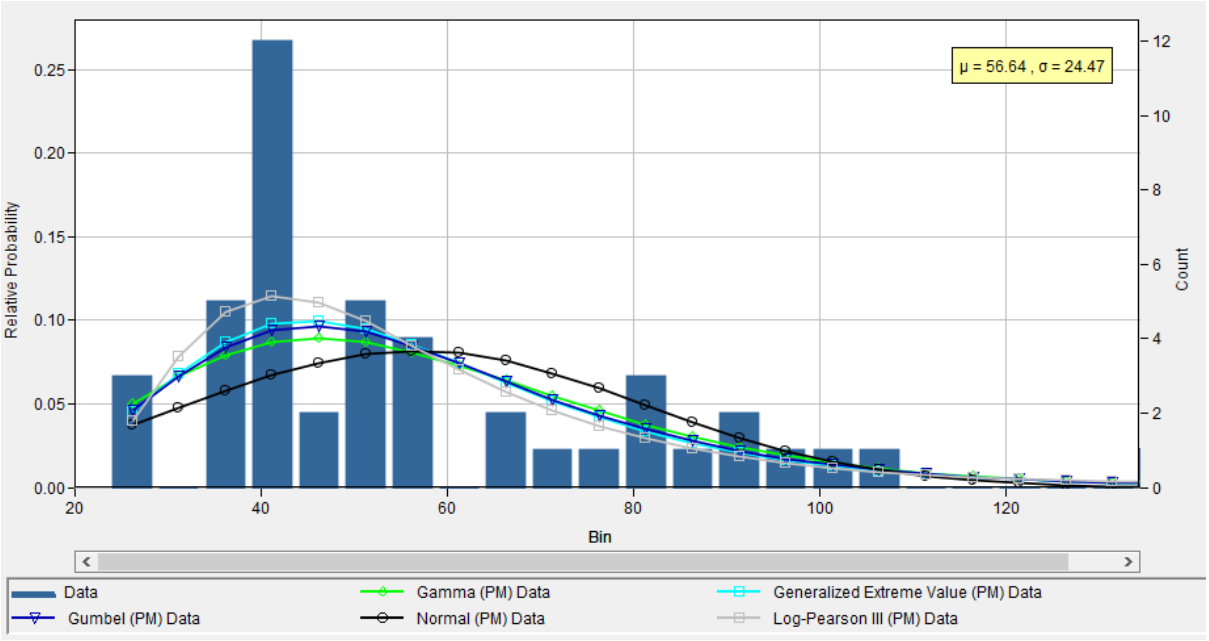

Figure 20: Distribution fitness test

The Log-Pearson Type III distribution is calculated using the following equations:

$$f(x) = \frac{((x-\tau)/\beta)^{\alpha-1} exp(-(x-\tau)/\beta)}{|\beta|\Gamma(\alpha)} \quad (8)$$

f (x) is the probability density function with $(x - \tau)/\beta \geq 0$, τ is the location parameter, α is the shape parameter, β is the scale parameter, and Γ (α) is the Gamma function.

$$logx = \overline{logx} + K\sigma_{logx} \quad (9)$$

$$\sigma_{logx} = \sqrt{\sum (logx - \overline{logx})^2/(n-1)} \quad (10)$$

$$C_s = n\sum (logx - \overline{logx})^3/(n-1)(n-2)(\sigma_{logx})^3 \quad (11)$$

x is the flood discharge value of some specified probability, $\overline{logx}$ is the average of the logx discharge values, K = frequency factor and σ_{logx}= the standard deviation of the logx values. Cs = skewness coefficient. The frequency factor K is a function of the skewness coefficient and return period that can be found using the frequency factor table (Beard, 1962).

Based on the above equations, the statistical information in Table 9 can be calculated and the flood magnitudes for the various return periods can be found as well. Further, the flood frequency curve is plotted in Figure 21.

Table 9: Statistics of annual maximum discharge from 1976-2021

Mean	Standard deviation	Skewness	Kurtosis
56.638	24.471	1.292	1.623

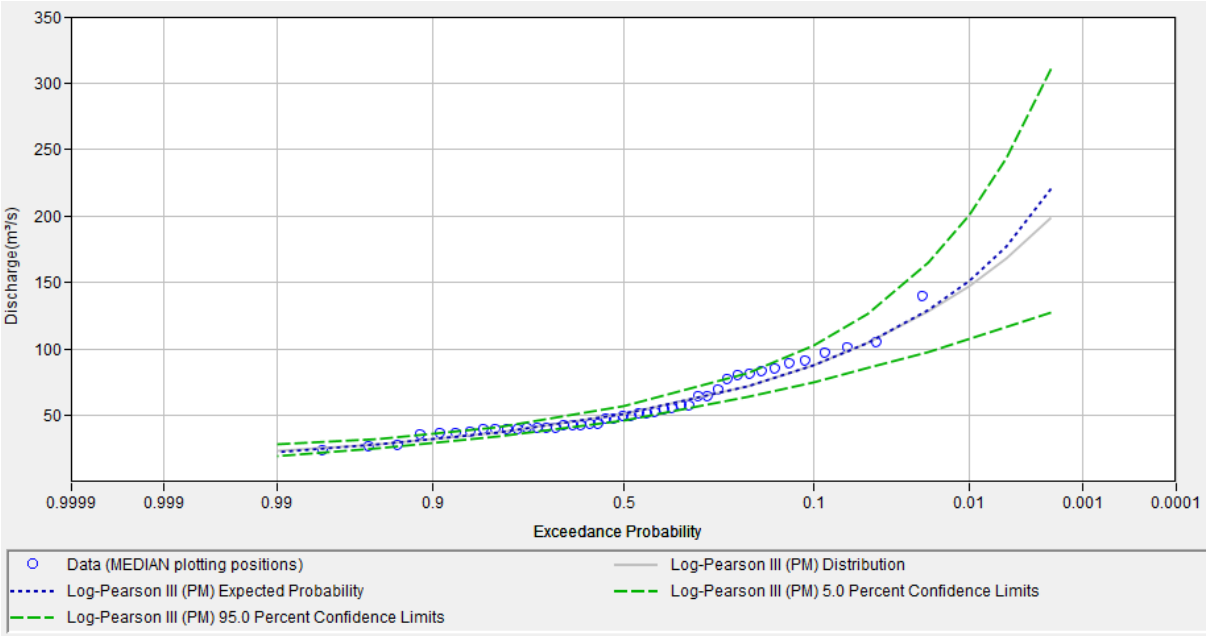

Figure 21: The Log-Pearson Type III plot for the prediction of the different return period flow

3.2 Methodology

Separate methods are used to represent each process of the rainfall-runoff generation in HEC-HMS, including the model of water loss, model of direct runoff, model of base flow, and reach routing. The basin model, meteorological model, and control specifications are combined with each simulation run in order to obtain the simulation results. The following methods in table 10 were selected for each process of runoff generation in the hydrological modelling.

Table 10: Selected methods in HEC-HMS

No.	HMS Process	Methods
1	loss	SCS Curve Number Method
2	Transform	SCS Unit Hydrograph
3	Base-flow	Recession
4	Reach Routing	Muskingum

3.2.1 SCS Curve Number Method

The Curve Number Method was originally developed by the Soil Conservation Service in the United States. Then, it has been adapted to conditions in other parts of the world. Some additional criteria for

regional research have been developed, while the basic concept is still extensively used all over the world. The Soil Conservation Service Curve Number method (SCS-CN) is an empirical method used for rainfall-runoff modelling. The dimensionless curve number has been used for estimating precipitation excess as a function of cumulative precipitation, soil cover, land use, and antecedent moisture. The major drawbacks of the method are sensitivity of the method to Curve Number (CN) values, fixing the initial abstraction ratio, and lack of clear guidance on how to vary Antecedent Moisture Conditions (AMC).

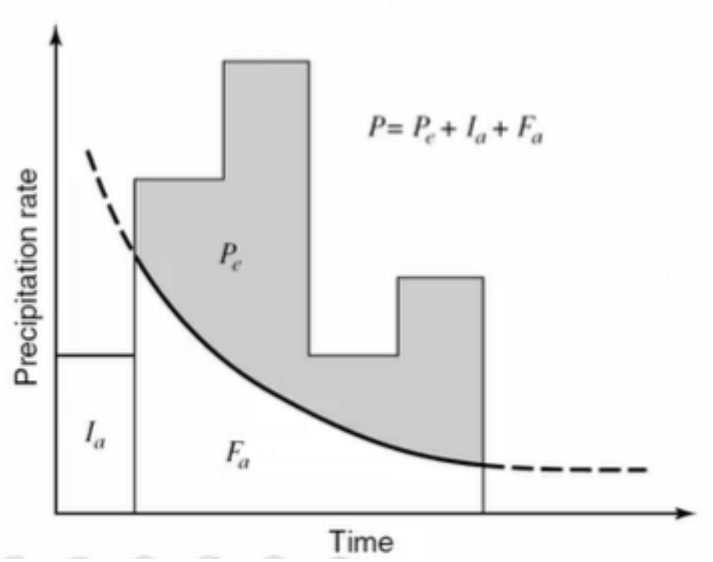

Figure 22: SCS Curve Number method (Scharffenberg, 2013)

Assumptions:

- The water loss from the total rainfall is used to satisfy the potential amount storage of S (or referred to as retention.
- F_a is the water reaching the ground detained by the watershed (mainly infiltrated water).
- The surface storage must fill up with rainfall (referred to as initial Abstractions, I_a) before any runoff generates. The initial abstraction (I_a includes water kept by evapotranspiration, infiltration, surface depression, and water intercepted by vegetation) (USDA, 1986).

$$I_a = 0.2S \tag{12}$$

- If no water is used to satisfy the soil storage after I_a, which will yield the maximum runoff.

$$P_e = P - I_a \tag{13}$$

- Ratio of the actual amount stored (F_a) to potential amount storage (S) is equal to the ratio of actual runoff to the maximum runoff.

$$F_a/S = (P - I_a - P_e)/S = P_e/(P - I_a) \quad (14)$$

Based on the above assumption until the accumulated rainfall exceeds the initial abstraction, the excess precipitation hence generates the runoff. The equation is as follows (eq. 15):

$$P_e = (P - 0.2S)^2/(P + 0.8S) \quad (15)$$

Pe = accumulated precipitation excess at time t; P = accumulated rainfall depth at time t; Ia = the initial abstraction (initial loss); and S = potential maximum retention.

The maximum retention (S) and watershed characteristics are associated with curve number (CN). Also, S is associated with the soil and land cover conditions of the watershed through the Curve Number (CN) varies in a range of 0 to 100. The relationship is given in Eq. (16).

$$S = (25400 - 254CN)/CN \quad (16)$$

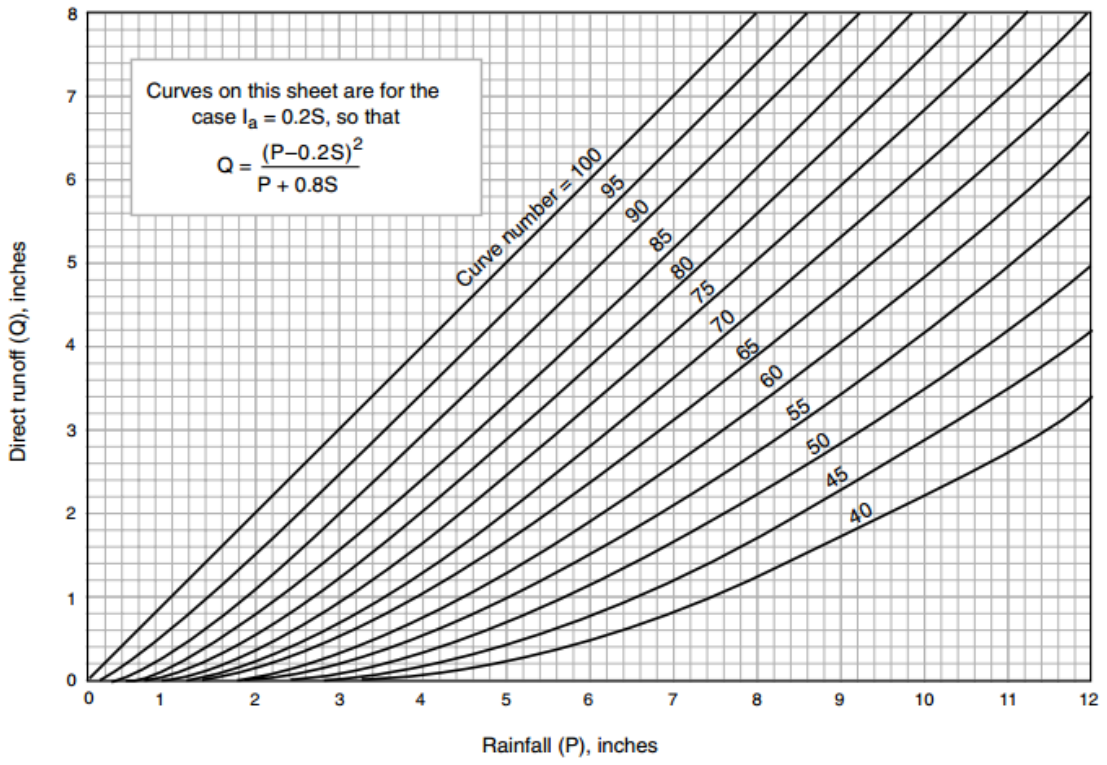

Figure 23: Solution of runoff equation (Cronshey, Roberts and Miller, 1985)

3.2.2 Transform Method

The conversion of precipitation into the runoff is conducted by the transform method within each subbasin and converges at the outlet. For the transform method, an SCS unit hydrograph is based on a dimensionless unit hydrograph and achieved by using the user-specified S-graph in table 11. Different graphs vary depending on the type of terrain. Steep terrain tends to produce higher and earlier peaks

and vice versa. only one parameter for each subbasin (the lag time) is required in the SCS unit hydrograph method. The lag time is defined as the length of time between the centroid of precipitation mass and the peak discharges of the resulting hydrograph (Scharffenberg, 2013). The X-axis consists of dimensionless time units and Y-axis consists of dimensionless discharge units in Figure 24. The relationship between the time of concentration (Tc) and the lag time (T-lag) is developed by equation (17). Further, the time of concentration is calculated by equation (18).

$$T_{lag} = 0.6 * T_c \quad (17)$$

T_{lag} = lag time.

$$Tc = (L)^{0.8} * (1000/CN - 9)^{0.7}/441Y^{0.5} \quad (18)$$

T_c= time of concentration, L= length of the mainstream to farthest divide, Y = average watershed slope%, CN= Curve Number.

Table 11: Different graphs for SCS unit hydrograph

General description	Peaking factor	Limb ratio (recession to rising)
Urban area, steep slope	575	1.25
Typical SCS	484	1.67
Mixed urban/rural	400	2.25
Rural rolling hills	300	3.33
Rural, slight slope	200	5.5
Rural, very flat	100	12

A typical dimensionless unit hydrograph consists of 37.5% of the total runoff volume before the peak and the remaining 62.5% volume after the peak discharge. A simplified form of the 'triangular' unit hydrograph is used to get the unit hydrograph (Figure 24). 37.5% of the volume on the left of Tp for the triangular unit hydrograph is assumed, then, T_b can be derived based on equation 19. It is known that the area under the unit hydrograph is equivalent to 10 mm. If the area of the watershed is in km^2 by using equation 21, it will end up with equation 22.

$$T_b = 1/0.375 \times T_p = 2.67T_p \quad (19)$$

T_b= base time, T_p = time of rising or time to peak.

$$T_p = \Delta t/2 + t_{lag} \quad (20)$$

Δt = the excess precipitation duration, t_{lag} = the basin lag, defined as the time difference between the centre of mass of rainfall excess and the peak of the UH.

$$1/2\ Q_p \times (2.67\ T_p) \times (3600) \ = \ 1/100 \times A \times 10^4 \quad (21)$$

A = area of the catchment.

$$Q_p = 2.08 \times A\ /\ T_p \quad (22)$$

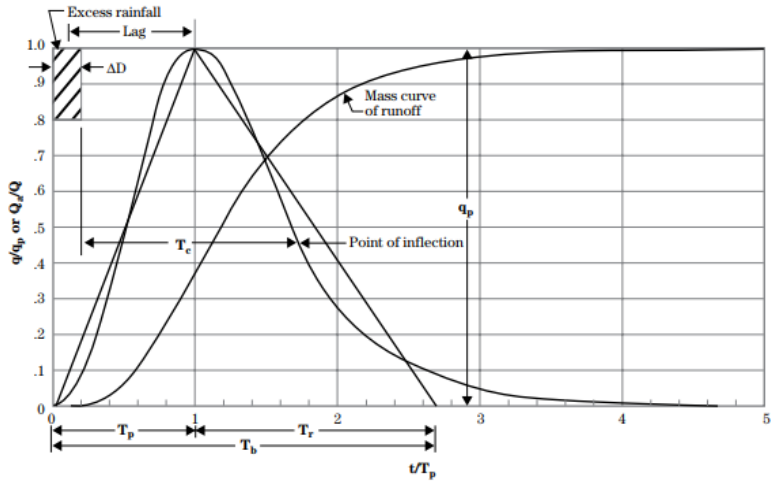

Figure 24: Curvilinear UH and equivalent Triangular DUH (Eslamian, 2014)

3.2.3 Reach Route Method

Muskingum method is used to route flow through the reaches. The observed rising channel storage during the increasing side and dropping channel storage during the falling side of a passing flood wave can be simulated by applying this method. The sum of prism and wedge storage is conceptualized as the total storage, as shown in Figure 25. Wedge storage is positive and added to the prism storage during the rising stage of the flood. On the contrary, during the falling stages on the receding side of a flood wave, wedge storage is negative and subtracted from the prism storage during the falling stages of the flood (Scharffenberg, 2013). The prism storage is expressed as the following equation:

$$S_t = K([XI + (1 - X)O]) \quad (23)$$

Where K and *X* are **Muskingum coefficients**, K is equivalent to travel time through the reach and *X* is the dimensionless weight given as $0 \leq X \leq 0.5$. The value of 0.0 will give maximum attenuation and 0.5 results in no attenuation. The initial value of X is 0.35 and will be calibrated later. I is the inflow rate and O is the outflow rate.

The cumulative storage in the system is obtained using the continuity equation with finite difference approximation below.

$$\left(\frac{I_{t-1}+I_t}{2}\right)-\left(\frac{O_{t-1}+O_t}{2}\right)=\left(\frac{S_t-S_{t-1}}{\Delta t}\right) \quad (24)$$

Storage-Discharge relationships (hysteretic) are described by the Muskingum routing procedure for systems. The relationship between storage and discharge at the outlet is not a unique relationship, it is looped. In addition, the Muskingum routing model can not simulate the backwater effect.

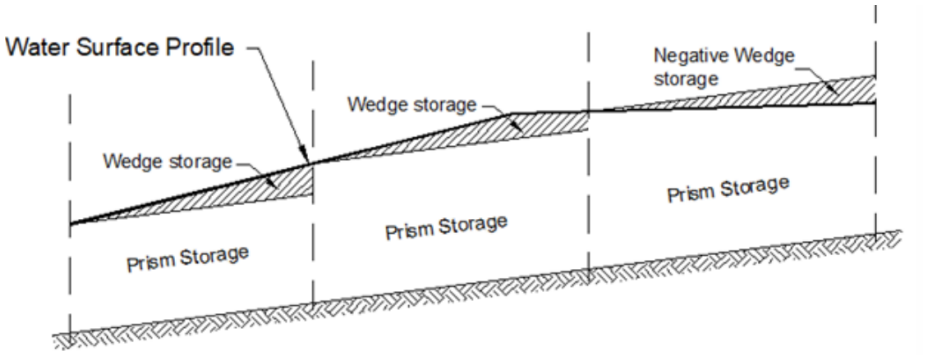

Figure 25: Wedge Storage (Eslamian, 2014)

3.2.4 Base Flow Method

Baseflow is a portion of runoff that is not directly generated from the excess precipitation during a storm event. In order to understand the hydrology process in a watershed, including the interaction of surface and subsurface water, the estimation of baseflow and direct runoff is needed. The recession base flow method is chosen in this study, which models the hydrograph's recession curve using the recession constant for specifying the rate at which recession flow drop with time. Baseflow can be separated from a total streamflow hydrograph by using a recession model based on the following relationship: the parameters **k, and t** are calculated by the following equation and the parameters can be adjusted during calibration.

$$Q_t = Q_0 k^t \quad (25)$$

Q_t = flow at time t, Q_0= flow at the beginning of the recession curve, k= exponential decay constant.

3.2.5 Snowmelt

Snowmelt runoff plays a significant role in the hydrological cycle in some watersheds. Generally, water is stored and accumulated as snow when the air temperature is negative. Snow is accumulated in a snowpack during the wintertime and transforms continually into ice crystals in response to diurnal temperature fluctuations. Hence, the amount of snowmelt is highly influenced by the various atmospheric conditions.

There are two conditions for melting, wet melt (in presence of rain) and dry melt (in absence of rain).

The water content of the snowpack is commonly measured by the snow water equivalent or SWE. The SWE is the depth of water obtained from melting a unit column of the snowpack.

The snowmelt method is included in the meteorologic model so it is only necessary while the air temperature is below the freezing point during a simulation. Currently, only the temperature index approach or degree-day method is available, which contains the conceptual representation of the snowpack energy.

$$M = C_m(T_a - T_b) \quad (26)$$

Where M= snowmelt in mm/d; C_m= the degree-day coefficient in mm/degree-day in °C; T_a= mean daily air temperature in °C; T_b= base temperature in °C.

The temperature index method in HEC-HMS simulates the liquid water stored at the soil surface that infiltrates as streamflow. This method has a fixed amount of snowmelt for each degree above freezing and includes a conceptual representation of the cold energy kept in the pack along with limited predefined conditions as well as other factors. The melt coefficient also varies as the snowpack's internal conditions and atmospheric conditions change.

A variety of parameter data of the temperature index method has to be assigned to each subbasin in Component Editor for the meteorologic model. Moreover, each subbasin must have at least one elevation band (from 1 to 10) and only one elevation band is selected due to the flattest plain across the catchment except the mountainous areas (2 bands). The following parameters need to be defined for modelling the snowmelt process.

Table 12: Initial parameters of snowmelt method

lapse rate (DEG C/1000m)	Represents the temperature change per 1000 meters. The lapse rate should be negative if the air temperature is cooler at high elevation than at low elevation. The initial value is -2.
PX temperature (°C)	Distinguishing between precipitation falling as rain or snow. Max value is 1.
Base temperature (°C)	The snowmelt amount is estimated by the difference between the air temperature and the base temperature melt rate and is multiplied by the melt rate. A typical value is 0.
Wet Melt rate (mm/°C-day)	The wet melt rate is used during the time when precipitation falls as rain, and the rainfall rate is higher than the rain rate limit. It is only applicable when it is raining. The initial value is 2.5.
Rain rate limit (mm/day)	The rain rate limit distinguishes between dry melt and wet melt. Rain rate exceeding this limit leads to computing wet melt and

	when the rain rate is less than the value given only dry melt is computed. The default value is 0.
ATI Coefficient	When the precipitation rate is less than the rain rate limit, the melt rate computation for the time steps starts with the antecedent melt rate index that demands a coefficient to update from one-time interval to the other. The default value of this coefficient is 0.98.
Constant rate	Meltrate is calculated by using a constant value.
Cold limit (mm/day)	Illustrate the rapid change in the temperature of the snowpack during high precipitation rates. When the precipitation rate is higher than the cold limit, the antecedent cold index is set to the temperature of the precipitation. If the temperature is above the base temperature then the cold content index is set similar to the base temperature else it is set to the actual temperature. If the precipitation rate is lower than the cold limit the cold index is computed as an antecedent index. A default value of 0 mm/day is applied.
Coldrate coefficient	Applied for updating the previous cold content index from one time step to the next. The default value is 0.5.
Water capacity (%)	Defines the amount of liquid water that has to accumulate in the snowpack before it turns into a surface runoff or infiltrates into the soil surface. Typically, ranging from 3-5 % of snow water equivalent.
Groundmelt method	Describe the snowpack accumulated above the only partially frozen or unfrozen ground melts by the heat transferred from warm ground. The constant value method is chosen.
Groundmelt (mm/day)	Constant value is used.|Inicial value is 0.

3.2.6 Hypothetical storm method

Recently, the Frequency Storm method was replaced by the Hypothetical Storm method and it is available in HEC-HMS version 4.2.1 and prior versions. It allows users to define the storm duration, depth, area reduction information, temporal pattern, and storm area. The Hypothetical Storm method includes a Component Editor with parameter data for all subbasins in the meteorologic model.

Assumptions:

- Each catchment receives the same amount of precipitation, and the rainfall is distributed uniformly in each subbasin.
- For large or hydraulically complicated basins, it may not be precise.

Four standards of SCS temporal patterns (SCS Type 1, SCS Type 1A, SCS Type 2, and SCS Type 3), a user-specified pattern, and an area-dependent temporal pattern are provided. The user-specified pattern is chosen since it is based on the practical hourly precipitation data and is more precise for the

specific region. The percentage curve is required and it should be normalized both on the x-axis (time %) and y-axis (precipitation %) in Figure 26.

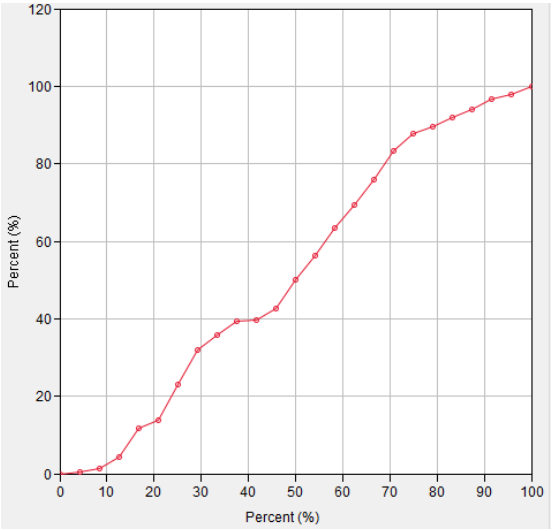

Figure 26: Percentage curve

For the storm duration, as long as it is longer than the time of concentration it can be applied for. Also, the frequency with 24 hours duration was used for the simulation. The area reduction function is also used in this method, as the storm area increases, the assumption of uniform rainfall in space is stretched. Afterwards, the area reduction analysis can be applied. The results will also be compared with the observed drainage area for different calibration points.

3.3 Control specification

Control specification is one of the major components of a project, although it does not include much parameter data. Their principal objective is to control when simulations start and stop, and what is the time interval being used in the simulation.

It works both for events and continuous simulation. In the basin model, the simulation is differentiated into an event or continuous simulation due to the time specified and the chosen method. The same interval can be used when viewing time-series results from the simulation. Sometimes, computations need to be carried out at a shorter time step and the results interpolated to the interval specified in the control specifications. Also, some parameters are sensitive to time intervals for the methods in the basin model. Those parameters should be estimated with knowledge of the time interval in the control specifications.

3.4 Model Evaluation

The model evaluation includes calibration and validation. The important parameters were analysed and used to determine the ones that can make a precise prediction of basin yield. Therefore, at first the model was run with the initial values, estimated by SCS-Curve number methods and output was collected. The output values were analyzed to determine their variations with respect to the base output set. In general, the observed peaks, timing, and volume should be reproduced.

Statistics used for model evaluation:

- Coefficient of Determination (R^2)
- Percentage Bias (PBAIS)

Coefficient of determination (R^2): It indicates the proportion of variance between the observed data and the simulation results.

R^2 =0, the model can not reproduce observations.

R^2 =1, the model can reproduce observations with no error.

0< R^2 <1, the extent to which the model reproduces observations.

$$R^2 = \left[\sum_{i=1}^{n} (Y_i^{obs} - \overline{Y}_{obs})\ (Y_i^{sim} - \overline{Y}_{sim}) / \sqrt{\sum_{i=1}^{n} (Y_i^{obs} - \overline{Y}_{obs})^2} \sqrt{\sum_{i=1}^{n} (Y_i^{sim} - \overline{Y_i^{sim}})^2} \right] \quad (27)$$

Where Y_i^{obs}= the observed flow (m^3/s); Y_i^{sim}= the simulated flow (m^3/s) and $\overline{Y}_{obs}$the mean observed flow (m^3/s) and $\overline{Y}_{obs}$ the mean simulated flow.

Percentage Bias (PBAIS): Measures the mean tendency of the simulated values to be larger or smaller than their observed ones.

- The optimal value of PBAIS is 0.
- Positive values present model underestimation bias.
- Negative values present model overestimation bias.

$$PBAIS = \left[\sum_{i=1}^{n} (Y_i^{obs} - Y_i^{sim}) * 100 / \sum_{i=1}^{n} (Y_i^{obs}) \right] \quad (28)$$

Quantitative Goodness of Fit criterion:

Table 13 Performance rating for evaluation metrics (Scharffenberg, 2013)

Performance rating	R^2	PBIAS
Very good	$0.65 < R^2 \leq 1.00$	$PBIAS < \pm 15$
Good	$0.55 < R^2 \leq 0.65$	$\pm 15 \leq PBIAS < \pm 20$
Satisfactory	$0.40 < R^2 \leq 0.55$	$\pm 20 \leq PBIAS < \pm 30$
Unsatisfactory	$R^2 \leq 0.40$	$PBIAS \geq \pm 30$

4. Simulation, Calibration, and Validation

4.1 Simulation Setup

The simulation describes how catchments and meteorology information are combined to simulate the hydrologic response. It works with terrain pre-processing, processing, basin and reaches processing, stream and sub-basins characteristics, Hydrological modelling system, etc. These processes will be discussed as follows.

Terrain preprocessing:

Once the terrain data is imported into the model, the process to refine the DEM and delineate the basin is preprocessing. The DEM processing can be applied both in QGIS and in HEC-HMS, in this study, it is accomplished by using HEC-HMS as some GIS functions are combined in the current version. The fill sinks feature was applied to modify the elevation value. Consequently, the water trapped in the cells is able to flow smoothly. Also, sinks in the cells were filled and a surface drainage pattern was formed.

Terrain Processing:

After the first step, the process of drainage runs the flow direction and flow accumulation processes. By applying this method, two new layers will pop up accordingly.

Flow direction: the flow direction for the grids is computed. Therefore, the grid has values assigned to each cell accounting for the direction of the steepest descent from that cell.

Flow accumulation: the flow accumulation grid accounts for the number of upstream grid cells. Each grid cell value is calculated by summing the total number of grid cells which flow into the grid cell. The stream network is formed with grid cells with great value and the grid cells of zero are situated at the topographic divide.

Streams identification: as a user-defined threshold. If the input cells with a greater value than the threshold are assigned value 1 else there is no data.

Outlet processing: generates the drainage point connected to the catchment.

Basin and reach processing:
Sub-basin elements and reaches elements can be merged. They have to be adjacent to each other. For reaches, an upstream-downstream relationship is needed. As long as the subbasins or reaches have a logical single outlet, the adjacent ones or upstream-downstream elements can be merged.

Stream and sub-basin characteristics:
Geospatial subbasin characteristics can be computed and stored in attribute tables within HEC-HMS. It consists of Basin slope, Basin relief, Basin centroid, Centroid flow path, River length, River slope, Longest flow path, centroid flow path, etc.

Hydrological modelling system:
After accomplishing the above processes, the model gains geographic information, hydrological elements and connections. Combined with the input data and model components, the simulation run can be conducted (Figure 27).

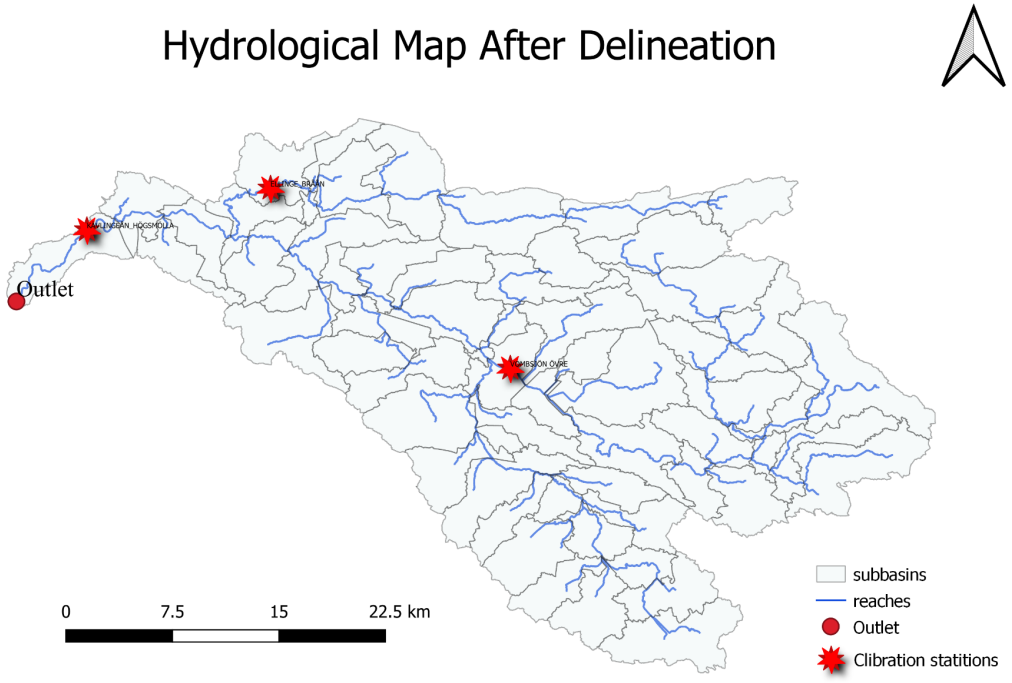

Figure 27: Hydrological map after delineation

4.2 Calibrations

In HEC-HMS, all the parameters were calibrated in order to reduce the error between the observed values and the simulated values in a couple of years (the highlighted years in Table 14). Also, the calibrations were implemented in wet years (over the average yearly flow), dry years (less than the average yearly flow), and normal years (close to the average yearly flow). In order to minimize the deviation between the observed and simulated values and to get the best set of parameters for calibrating and validating, the process can be accomplished either by manual adjustment of the parameters or automatically by using the iterative computation called optimization. Daily precipitation and discharge data from October to March of the next year during the normal year (2014 -2015) and dry years (2018-2020) were used for model calibration whereas the data during wet years (2007-2008) were used for validation. After calibration, the identical parameters will be used for validation and climate change modelling. Therefore, the flood hydrographs of the catchment with different scenarios were produced.

Table 14: Yearly water flow from maximum to minimum 1996-2020

No.	1	2	3	4	5	6	7	8	9	10	11	12	13
Flow	**6722**	5337	5169	4939	4938	4911	**4468**	4164	4096	**3883**	**3818**	3624	3525
Year	**2007**	2002	1998	2011	1999	2006	**2008**	2017	2000	**2015**	**2014**	2012	2004
No.	14	15	16	**17**	18	19	20	21	**22**	23	24	25	
Flow	3335	3316	3174	3071	3056	**3050**	**2901**	**2853**	2512	2369	2220	1978	
Year	2005	2001	2010	2013	2016	**2020**	**2019**	**2018**	1997	2009	1996	2003	

The optimization tool was used to calibrate the model parameters in HEC-HMS. Firstly, all parameter ranges (minimum to maximum) should be set in order to guarantee reasonable parameter values are identified during the iterative process. Also, the process of water generation and transport within subbasins and the process of water transport in rivers are simulated. Thus, parameters, such as basin and reach elements such as initial abstraction (I_a), curve number (CN) and Lag time (LT), recession constant, ratio to peak, Muskingum K and X, were calibrated automatically by optimization trials. The resultant output hydrographs were computed at Högsmölla (outlet) , Ellinger and Vombsjön. Minimization of the difference between computed and observed discharge is set as the goal of optimization. Finally, the parameters were adjusted manually until a satisfactory result was obtained for the sub-basin.

The whole catchment includes 61 sub-basins in total, only some of the catchments will be represented in the calibration process (Table 15). While the catchments selected should cover most parts of the catchment.

Table 15: Initial and Calibrated values for each sub-basin

Subbasins No.	Initial abstraction (mm)		Curve number		Lag time (mins)	
	Input	Optimized	Input	Optimized	Input	Optimized
20	12.35	47.13	80.45	38.11	155.62	251
9	15.45	29.39	76.68	91.16	263.23	400
98	11.28	36.78	81.82	73.26	176.59	450
4	19.95	40	71.81	75.74	235.21	450
6	16.45	45	75.54	70	204.95	398
14	20.31	2	71.44	75.06	168.99	1
27	18.98	70	72.80	65	149.72	450
28	16.58	68	75.39	69.16	237.80	455
33	12.12	1	80.74	77.34	228.02	455
101	11.61	70	81.40	73.54	103.00	450

Table 16: Initial and optimized parameter values for Muskingum equation

Reach No.	Muskingum K（hr）		Muskingum X	
	Input	Optimized	Input	Optimized
11	1.5	45.54	0.35	0.3
12	2.3	144	0.35	0.3
13	1.3	25.26	0.35	0.3
14	1.8	149.98	0.35	0.3
15	3	87.95	0.35	0.3
16	1.73	4.16	0.35	0.3
17	2.5	102.76	0.35	0.3
18	1.2	14.92	0.35	0.3
19	2.5	118.31	0.35	0.3
20	1.1	4.5	0.35	0.3

The model is more sensitive to the above parameters that are adjusted during calibration. Initially, the computed volume is more than the observed value and the computed peak flow is also higher than the observed flow in Figure 28. Accordingly, an expectation of decreasing the volume and reducing the peak flow is made.

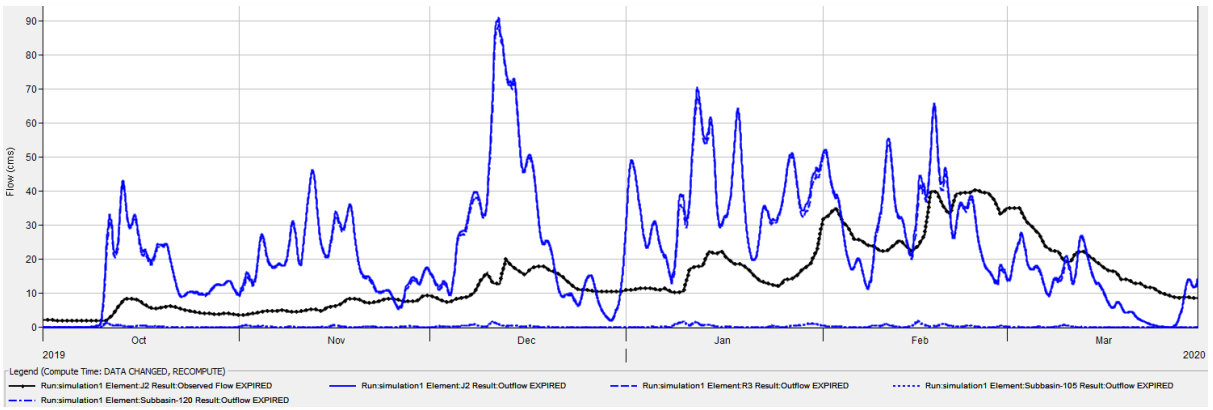

Figure 28: The initial hydrograph before calibration

Decreasing the computed volume and the peak flow:

It can be observed that most of the initial abstraction values were decreased, which implies more water will infiltrate or be intercepted in the model. Also, a longer lag time is required in most cases, which accounts for more travel time within sub-basins. The slope over the catchment is flat, none of them is over 5%, which may explain the reason for more travel time.

For the reach routing, Muskingum K values were increased, which means more travel time is demanded as well. Muskingum X parameter varies between 0 to 0.5. When X = 0, it means maximum attenuation, and when X = 0.5, there is only translation. In this study, X parameters are decreased from 0.35 to 0.3, which implies more attenuation. The parameters of the temperature index method for snowmelt are allocated with mostly default values in HEC-HMS. Only the melt rate is varied from 3 to 2.5.

4.3 Validation

The validation period was from the 1st of October 2007 to the Mar 31st of 2008 during the wet year. All parameters remain the same as the values in the calibration.

5. Results

5.1 Calibration

The calibration In HEC-HMS is implemented at three stations (*Ellinge, Högsmölla and Vombsjön*) from 1st October to 31st March in different years. The model calibrations were conducted under a normal year (close to the average), and a dry year (below the average) respectively. Then, the validation will be carried out in wet years (above the average). The time period (1st October to 31st March)is chosen since the peak flow is more significant based on the discharge data analysis. The time period from 2014 to 2015 for the normal year and the time period from 2018 to 2019, 2019 to 2020 for the dry year were selected during calibration. The solid blue line indicates the computed flow (including the direct runoff and baseflow) and the orange line indicates the observed flow from figures 29 to 37. Further, the differences in peak flow, time of peak and volume were analyzed.

As discussed in chapter 4.2, both manual and optimized methods were used (Tables 14 and 15) in order to get a satisfactory peak discharge, total volume and time to peak. It can be observed that the optimized graphs gave close agreement to the observed hydrograph. Also, according to the criteria, almost all of the results are within the acceptable range except for the result at Vombsjön.

5.1.1 Calibration during the normal years 2014- 2015

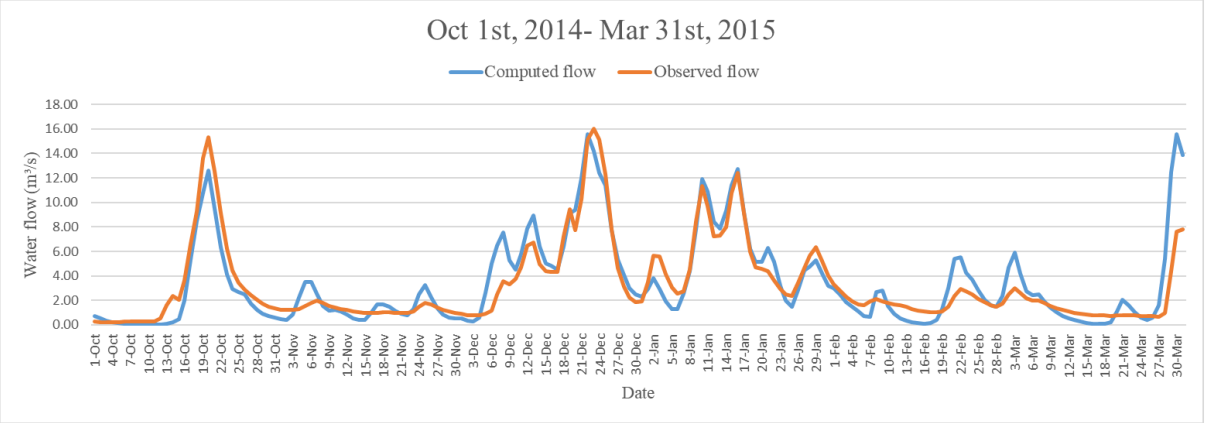

Figure 29: Result of calibration at Ellinge during the normal year

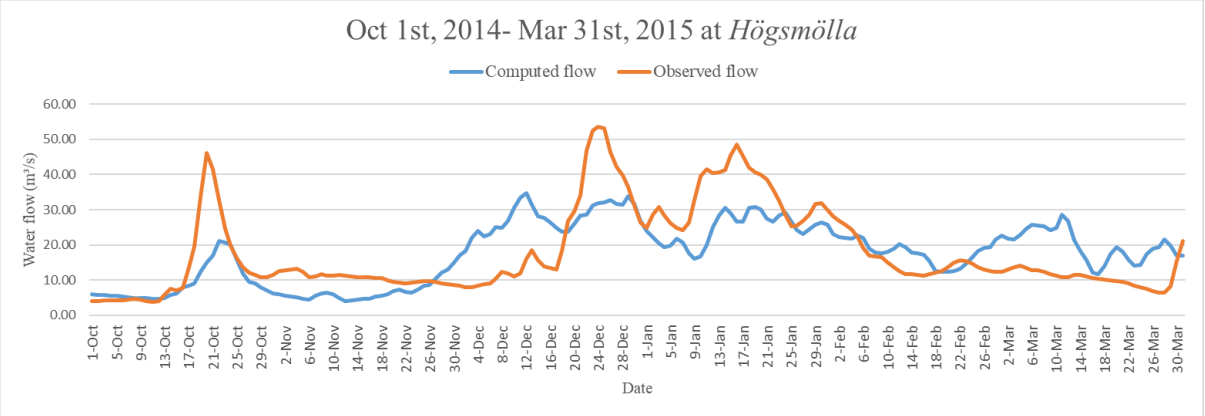

Figure 30: Result of calibration at Högsmölla during the normal year

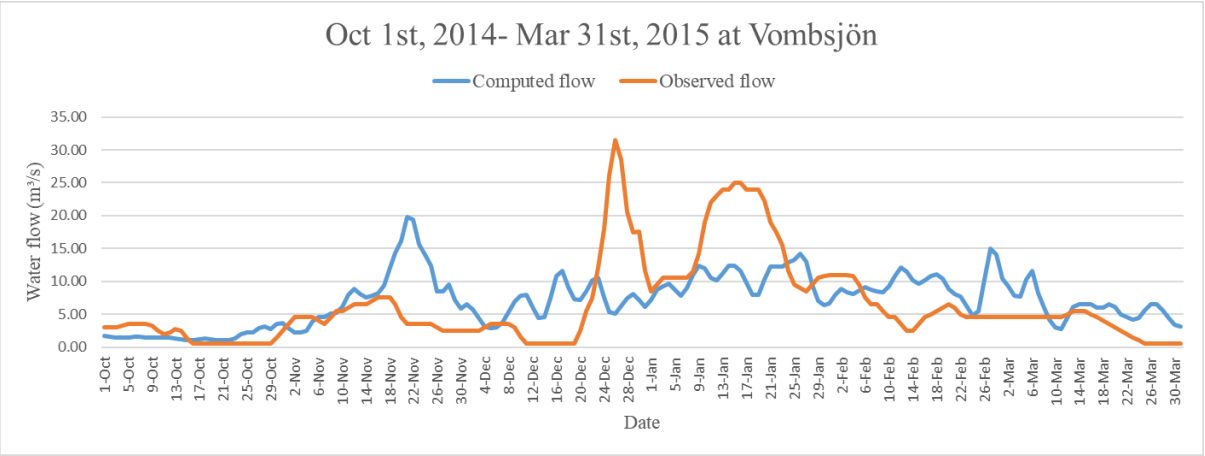

Figure 31: Result of calibration at Vombsjön *during the normal year*

Table 17: Comparison of peaking time, Magnitude, Volume between observed and computed flow 2014-2015

Calibration points	Peaking time			Magnitude (m³/s)			Volume (mm)		
	Observed	*Computed*	Δ(D)	Observed	*Computed*	Δ(%)	Observed	*Computed*	Δ(%)
Ellinge	20Oct	20Oct	0.5	16.8	16.5	-1.7	346.72	337.2	-2.8
Högsmölla	14Dec	25Dec	1	57	35.7	-35	248.95	253	+1.8
Vombsjön	22 Nov	26Dec	34	35.2	21.1	-66	253	277	+9.4

5.1.2 Calibration during the dry years 2018-2019 and 2019-2020

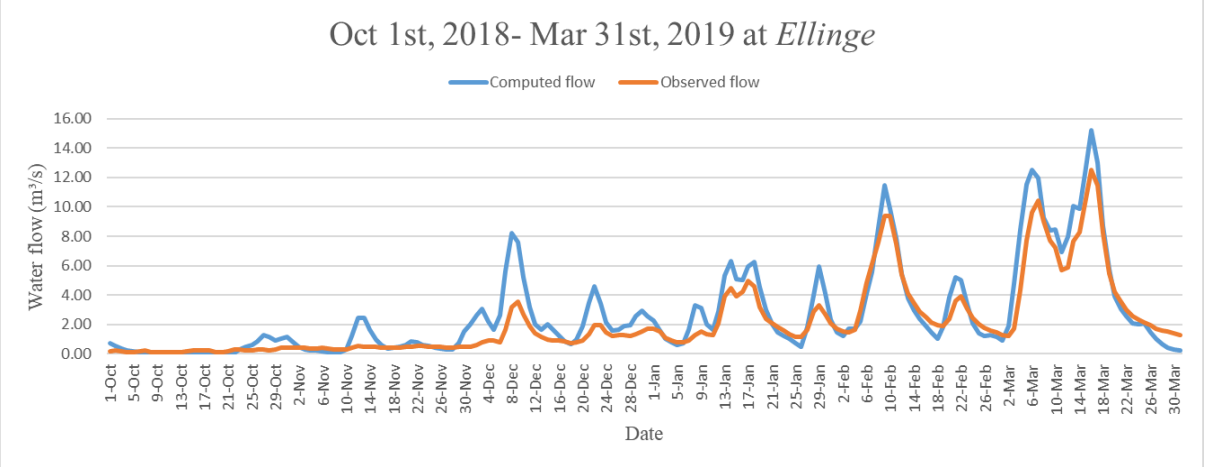

Figure 32: Result of calibration at Ellinge during the dry year

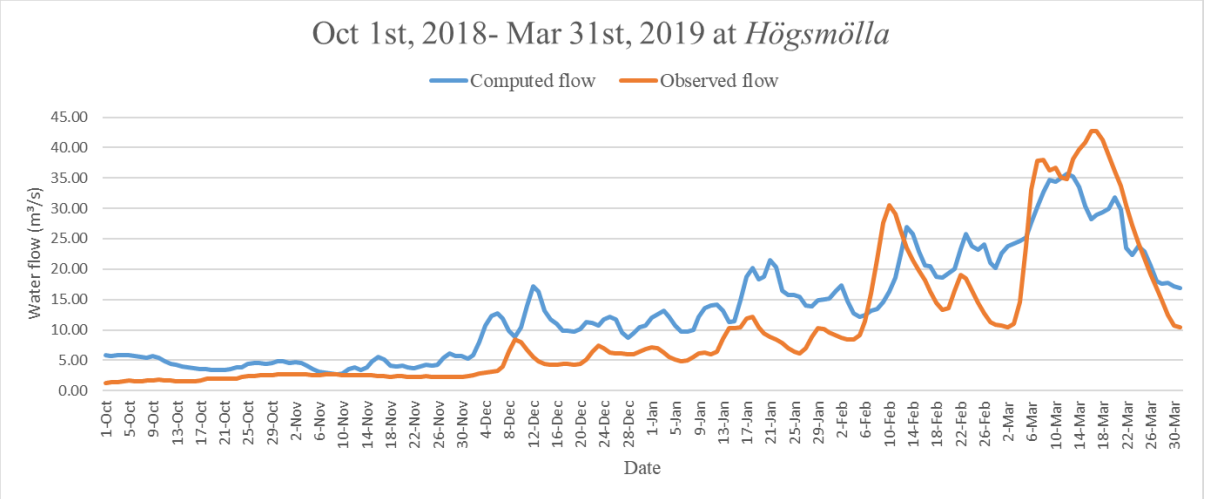

Figure 33: Result of calibration at Högsmölla during the dry year

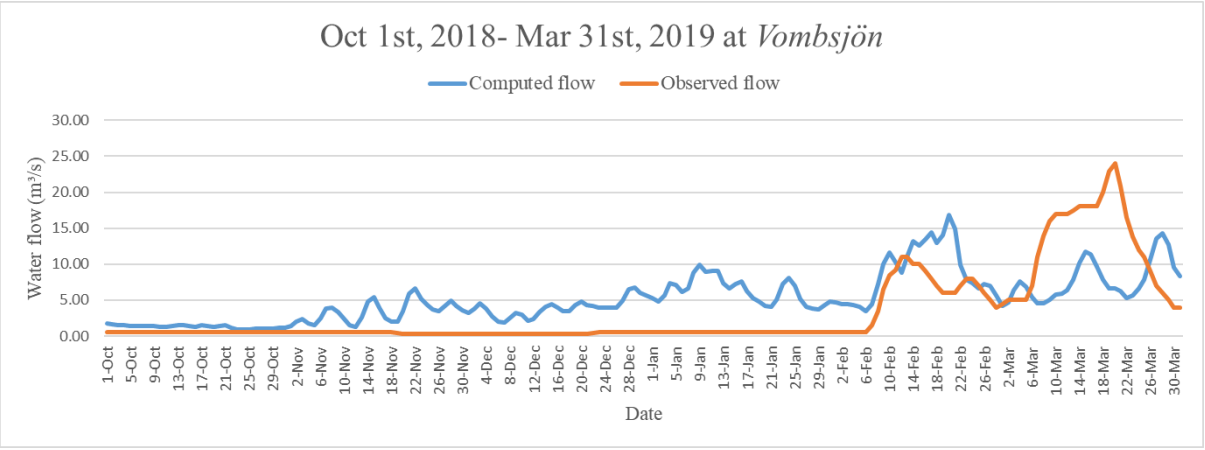

Figure 34: Result of calibration at Vombsjön during the dry year

Table 18: Comparison of peaking time, Magnitude, Volume between observed and computed flow 2018-2019

Calibration points	Peak time			*Magnitude (m^3/s)*			*Volume (mm)*		
	Observed	*Computed*	Δ(D)	Observed	*Computed*	Δ(%)	Observed	*Computed*	Δ(%)
Ellinge	*17Mar*	*16Mar*	*1*	*12.8*	*15.5*	*+17*	*223.95*	*281.55*	*+20*
Högsmölla	*17Mar*	*12Mar*	*5*	*43.1*	*35.9*	*-16*	*144.66*	*187.07*	*+22*
Vombsjön	20 Mar	20 Feb	30	24	17.1	40	129	202	+56.9

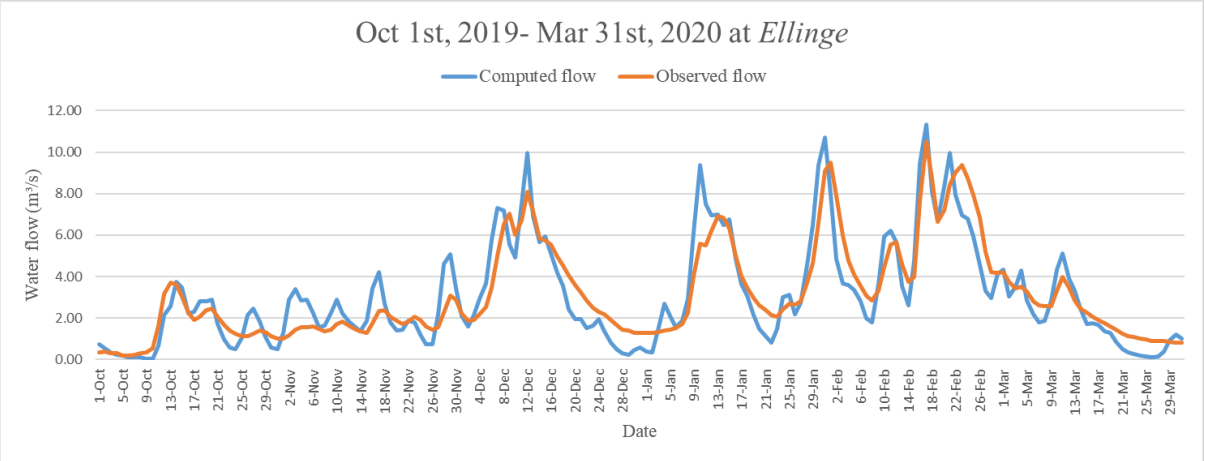

Figure 35: Result of calibration at Ellinge during the dry year

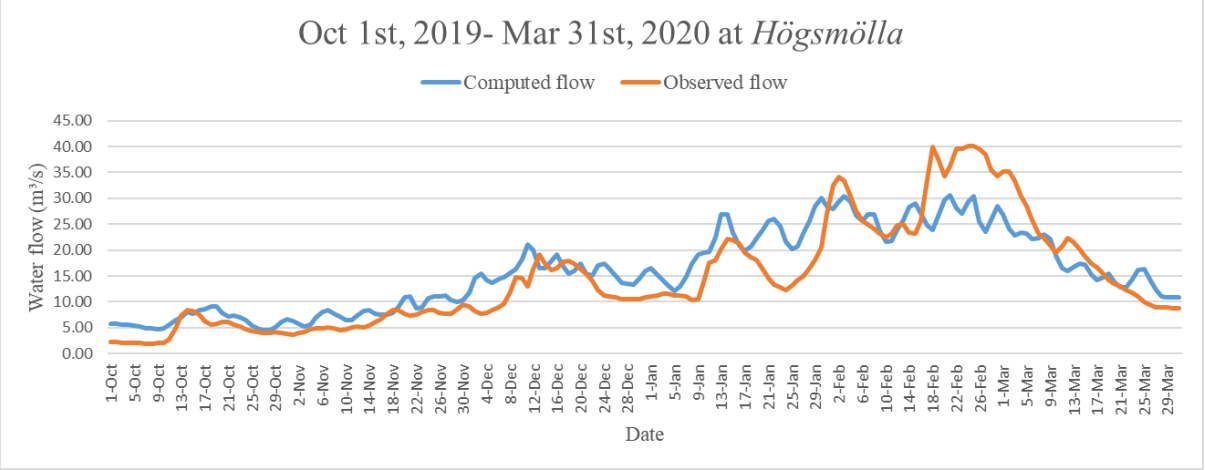

Figure 36: Result of calibration at Högsmölla during the dry year

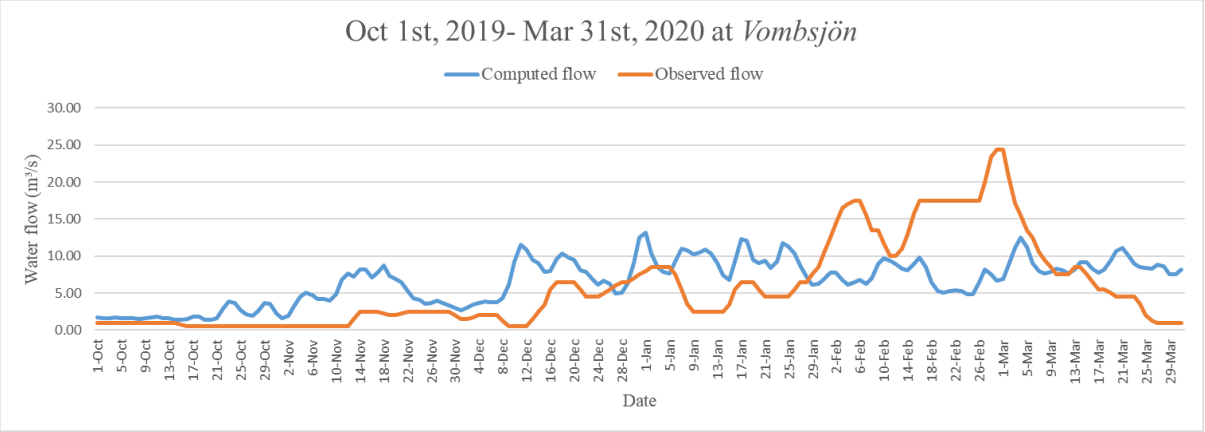

Figure 37:Result of calibration at Vombsjön *during the dry year*

Table 19: Comparison of peaking time, Magnitude, and Volume between observed and computed flow 2019-2020

Calibration point	Peak time			*Magnitude (m³/s)*			*Volume (mm)*		
	Observed	*Computed*	Δ(D)	Observed	*Computed*	Δ(%)	Observed	*Computed*	Δ(%)
Ellinge	*17 Feb*	*17 Feb*	*0.2*	*10.8*	*11.9*	*+9*	*320.67*	*326.16*	*+1.7*
Högsmölla	*25 Feb*	*25 Feb*	*0.2*	*40.6*	*31.4*	*-22*	*225.39*	*208.65*	*-8*
Vombsjön	*29 Feb*	01 Jan	58	12.7	14	+10	228.92	258.13	+12.7

All hydrographs of simulated outflow and observed flow were showed at above Figures during the calibration period. There was a close similarity of trend between the simulated and observed hydrograph. Also, the peak time occurred almost at the same time. The computed peak flow at Ellinge matches well with the observed flow and the computed maximum flow was about 16.6 m³/s.While the peak of the hydrographs at *Högsmölla* was generally less than the peak of observed hydrographs and the computed maximum flow was about 35.9 m³/s. This might be the fact that watershed physical characteristics variation, 2% of the land use is changing (Vattenrådet – Kävlingeån, 2022). As well as this, the SCS-curve number method is a simplified method used to estimate the soil moisture, which may not reflect actual soil moisture content.

It also can be observed that all computed peak flow and volume at Vombsjön do not match the observed flow since the flow at Vombsjön is regulated. The observed flow keeps almost constant from October to the start of February in Figure 34. As well as this, based on the precipitation analysis, the heaviest precipitation used to occur between August and October while the peak flow often occurred during February or March due to the Vombsjön lake buffering.

The results were in the acceptable range according to evaluation criteria except for Vombsjön. It recommended that the relative percent errors between the observed and simulated values should be below ±30%. Most of the results can be considered good fitness, the result of calibration at Högsmölla

during the time 2018-2019 is considered satisfactory according to the evaluation criteria. The negative values indicated model underestimation bias while the positive values of percent error indicated model overestimation bias.

5.2 Validation

In order to verify the output of the model, Validation was also conducted at the same station as calibration from 2007 to 2008.

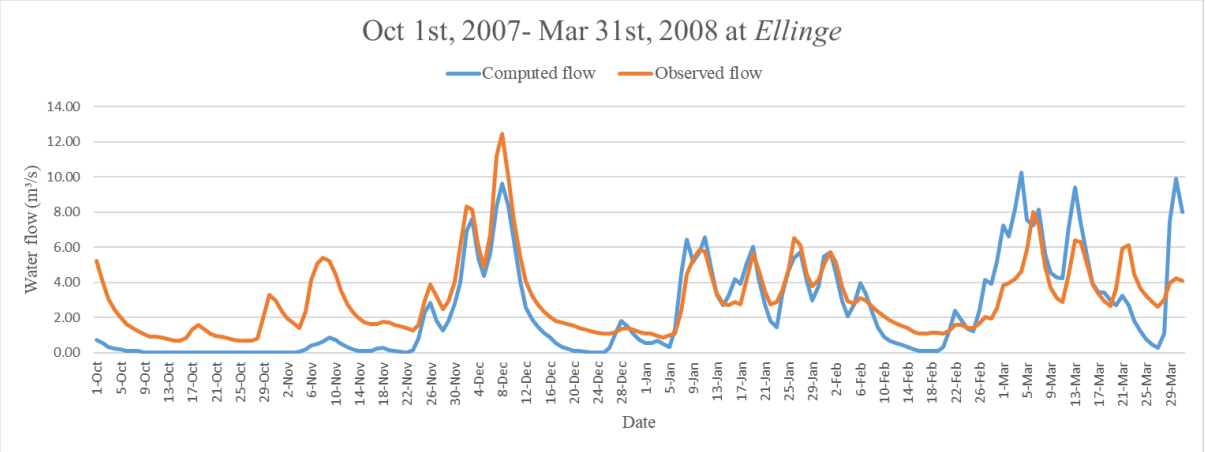

Figure 38: Result of validation at Ellinge during the wet year

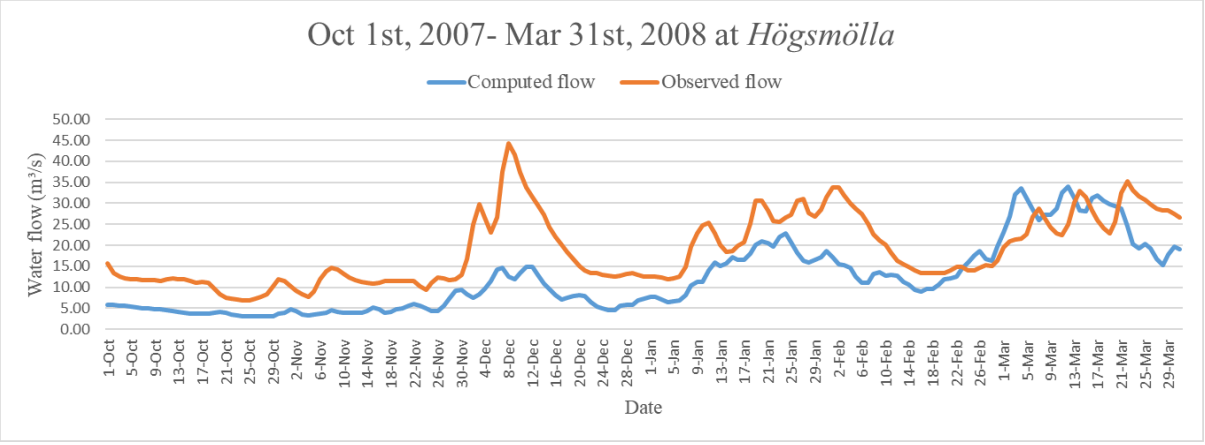

Figure 39: Result of validation at Högsmölla during the wet year

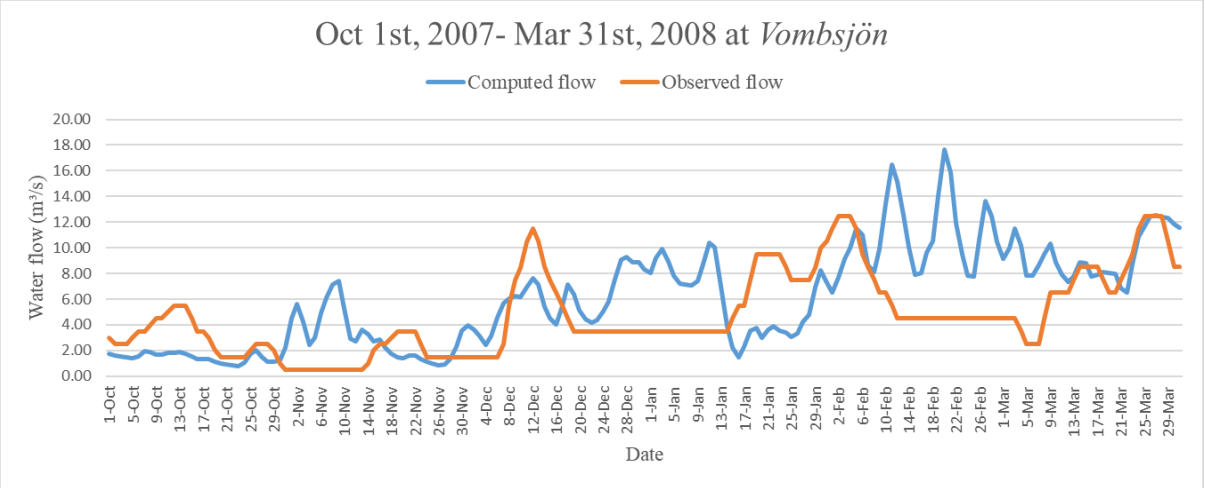

Figure 40: Result of validation at Vombsjön *during the wet year*

Table 20: Comparison of peaking time, Magnitude, Volume between observed and computed flow 2007-2008

Validation point	Peak time			*Magnitude (m³/s)*			*Volume (mm)*		
	Observed	*Computed*	Δ(D)	Observed	*Computed*	Δ(%)	Observed	*Computed*	Δ(%)
Ellinge	*8Dec*	*30Mar*	*112*	*13.7*	*11*	*-19*	*316.85*	*243.37*	*-23*
Högsmölla	*8Dec*	*12Mar*	*100*	*45*	*34.3*	*-23*	*266.1*	*171.01*	*-35*
Vombsjön	*12Feb*	*20Feb*	*8*	*12.5*	*17.9*	*+31*	*188.38*	*236.38*	*+25.5*

The hydrographs during the validation period are presented in Figures 38-40. A similarity in the trend of simulated and observed hydrographs can be visualized except for the ones at Vombsjön. It can be also observed that simulated flow was generally less than observed flow in wet years. The time of peak shift greatly as well but the peak discrepancies were still within the range. The computed maximum flow at Ellinge and Högsmölla was about 11 m³/s and 34.3 m³/s respectively. It may due to the fact that the curve numbers in the normal years are relatively lower than the wet year, which may not reflect the actual soil moisture content.

5.3 Model Evaluation

The summary statistics for all observed flow at different locations were used in the simulation, which includes Coefficient of Determination (R^2), and Percent Bias (PBIAS) in table 20. According to the evaluation criteria, different colours show the extent of good fitness. Green represents very good or good fitness, yellow indicates satisfactory while red represents unsatisfactory.

Table 21 shows most statistics information at Vombsjön is unsatisfactory due to the regulated flow from Vombsjön lake so it will not be discussed further. Most peak flow errors at the other two stations are close to the observed flood peak and within the acceptable limit of 30% which were clearly demonstrated. The maximum flow occurred between October and March of the next year in the

calibration and validation period. The computed maximum flow at Högsmölla (close to the outlet) was around 35.9 m³/s. For the volumetric error, the total discharge volume was close to the observed volume and within the acceptable range of 30% except for the one at Högsmölla in 2007-2008. Besides, All R^2 for calibration and validation period vary in the range of 0.4-0.9 which were also satisfactory. The diagrams of the maximum and the minimum of R^2 are displayed in Figures 41. a and 41. b, the rest diagrams were displayed in the appendix.

Table 21: Evaluation of the model calibration and validation statistics

No.	Computation Points	R^2	Pbias (%)	Peak error (%)	Year
Calibration	Ellinge, Oct 1,2014-Mar 31,2015	0.8	2.8	1.7	Normal year
	Högsmölla, Oct 1,2014-Mar 31,2015	0.4	-1.8	35	
	Vombsjön, Oct 1,2014-Mar 31,2015	0.13	9.4	66	
	Ellinge, Oct 1,2018-Mar 31, 2019	0.9	25	17	Dry year
	Högsmölla, Oct 1,2018-Mar 31,2019	0.78	29	16	
	Vombsjön, Oct 1,2018-Mar 31,2019	0.25	57	40	
	Ellinge,Oct 1,2019-Mar 31,2020	0.81	-1.7	*9*	
	Högsmölla,Oct 1,2019-Mar 31,2020	0.78	8	*22*	
	Vombsjön, Oct 1,2019-Mar 31,2020	0.12	12.7	10	
Validation	Ellinge,Oct 1,2007-Mar 31,2008	0.62	-23	*19*	Wet year
	Högsmölla, Oct 1,2007-Mar 31,2008	0.47	-35	*23*	
	Vombsjön, Oct 1,2007-Mar 31,2008	0.18	25.5	*31*	

Note: Green = very good or good-of-fitness, yellow = satisfactory, red = unsatisfactory

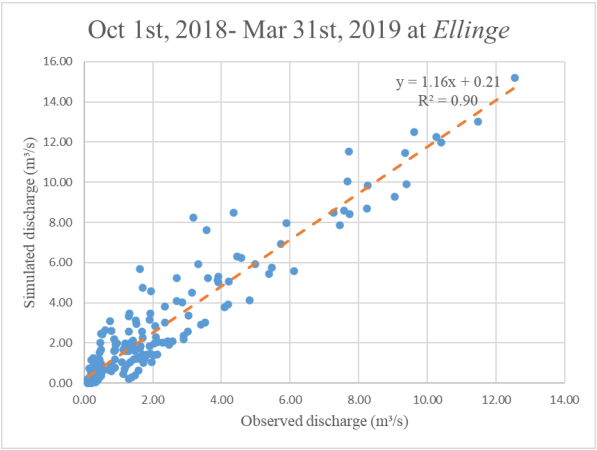

Figure 41.a: Maximum value of R^2

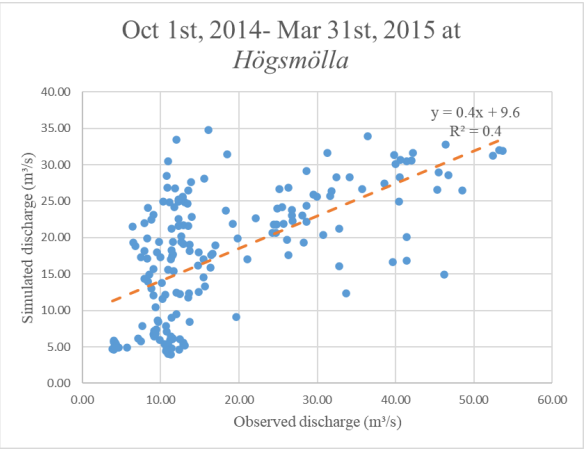

Figure 41.b: Minimum value of R^2

5.4 Results of Hypothetical Storm

The extreme event-based simulations were conducted by using a hypothetical storm method. Based on the precipitation frequency analysis in Table 22, the extreme rainfall event is converted into various return periods such as 2, 5, 10, 50 and 100 years for 24 hours duration. The hypothetical storm method assumes that the entire catchment will receive the same amount of designed rainfall. The control specification is added with start and end date-time. Finally, the basin model, meteorological model, and control specification are combined before running the simulation.

Table 22: precipitation frequency analysis

Return period (Years)	2 years	5 years	10 years	25 years	50 years	100 years
Precipitation (mm)	29.35	40.76	49.09	58.5	66.38	77.82

As we know that the parameters in the model were calibrated and validated during the continuous simulation. Therefore, all parameters can be put into use directly for storm event simulation. In this study, 24 hours storm is simulated with various return periods at Högsmölla (close to the outlet).

The generated peak discharge of various return periods during the extreme rainfall events is shown in Figure 42. It can be observed that the computed peak flow with the hypothetical method is much lower than the peak flow calculated by the historic data. It may be due to the fact that the hypothetical method assumed all subbasins received the same amount of precipitation and the precipitation boundary fit exactly the same as the shape of the catchment. Also, this method fits better for the small catchment or downscaling area.

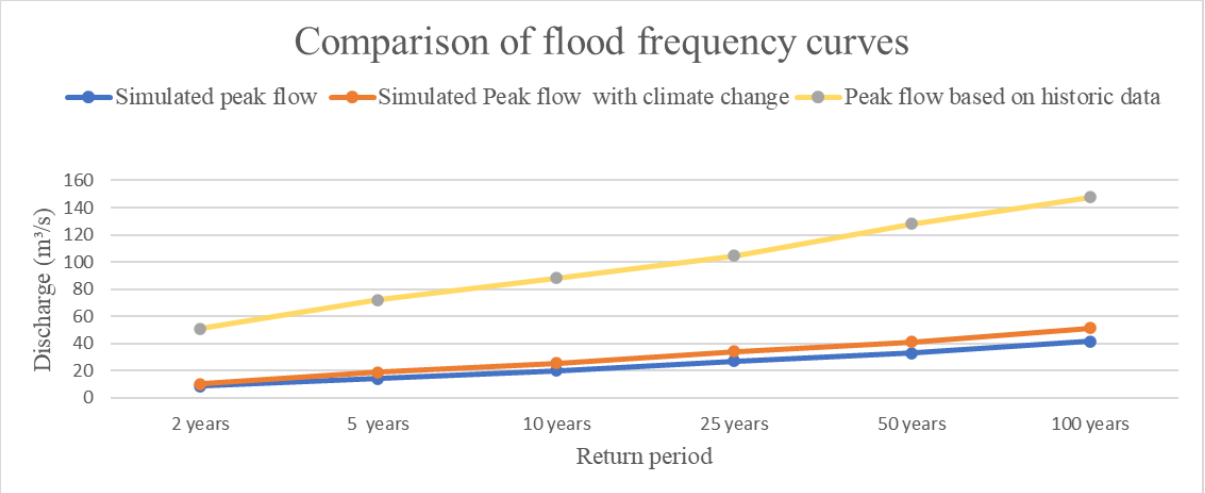

Figure 42: Comparison of flood frequency curves

It is also interesting to notice that the peak flow at Högsmölla (close to the outlet) for a return period of 100 years is 41.7 m^3/s, while the maximum flow in subbasin 12 is about 140 m^3/s in Figure 43.

Since there are no observation stations at subbasin 12, the comparison of discharge at subbasin 12 could not be discussed.

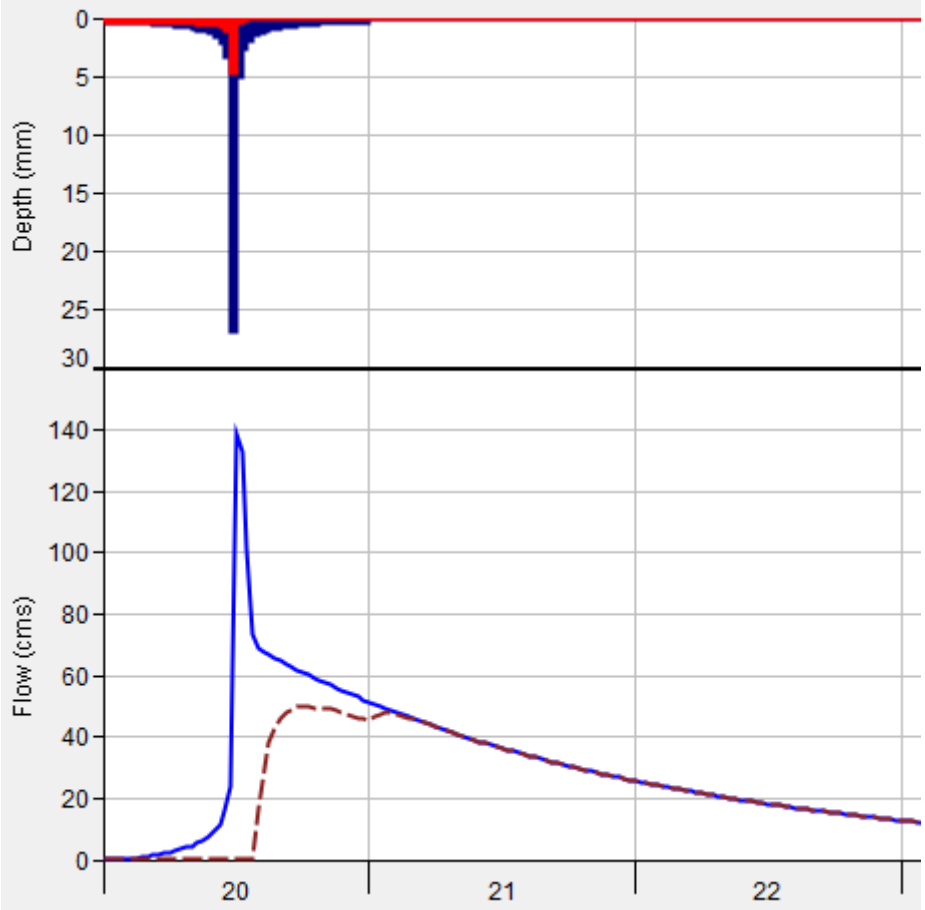

Figure 43: Hydrograph of 100 years return period at subbasin 12

5.5 Assessment of Impacts of Climate Change

The predicted increases in temperature and precipitation with climate scenario RCP 8.5 were simulated in the HEC-HMS model, which led to a rising runoff as well as rising peak flow as seen in Figure 44 to 46. The graphs compared the simulation results during 2019-2020 with the adapted climate scenario in 2094-2095 at the three computation points Ellinge, Högsmölla and Vombsjön.

Overall, the Figures show flow trends look much similar. Only a few changes during the first month, then the gap increases with time. For the climate change scenario, there is a slightly larger amplitude that is most likely caused by the increased precipitation and temperature. Also, there is an approximate 12% increase in peak flow at Ellinge, a 24% increase at Högsmölla and a 20% increase at Vombsjön respectively.

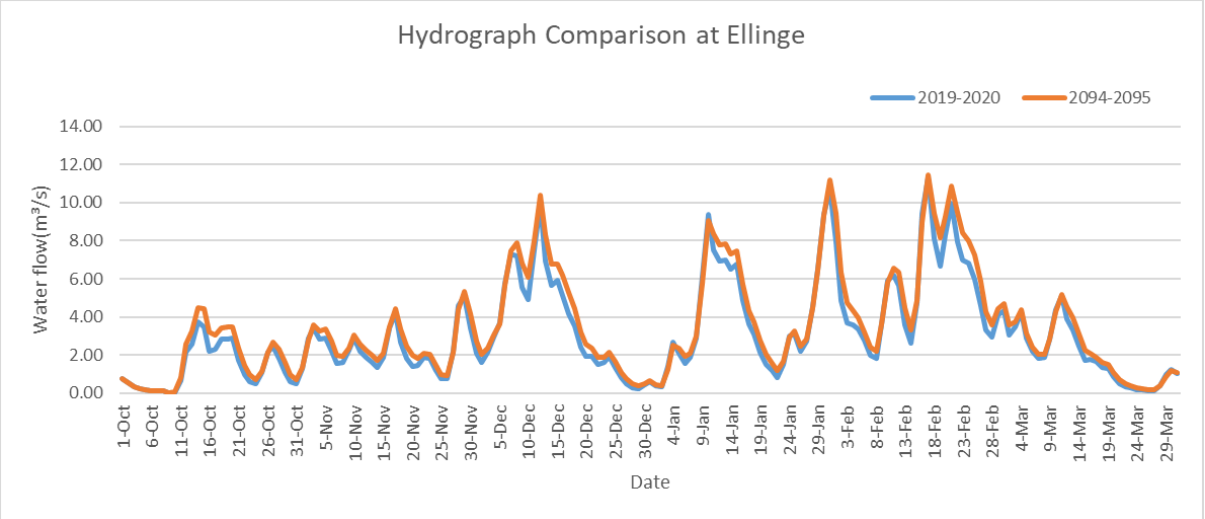

Figure 44: Daily peak flows comparison between 2019-2020 and 2094-2095 at Ellinge

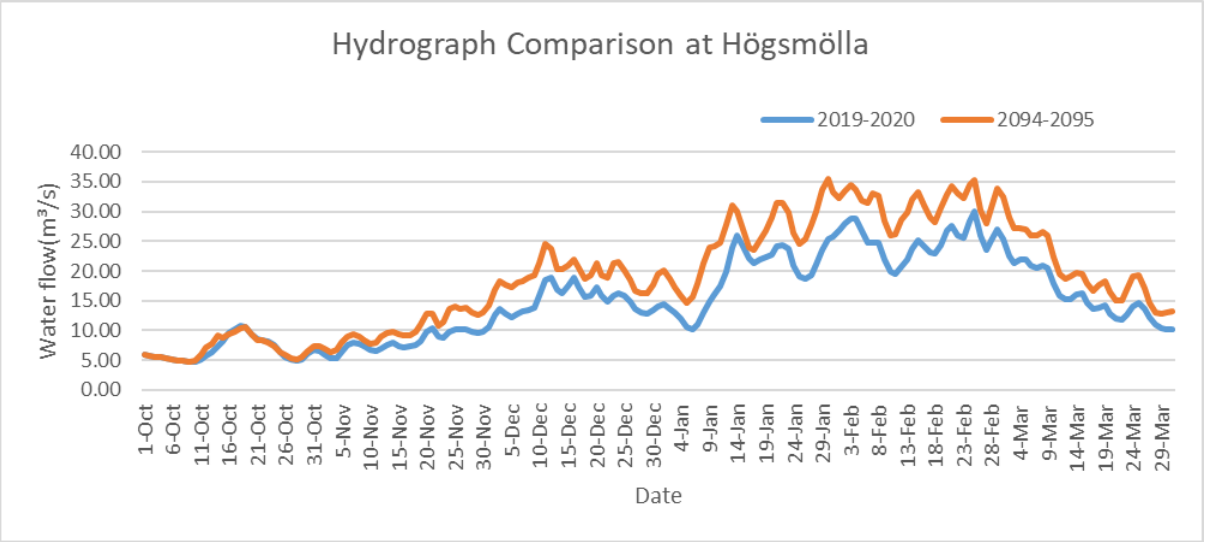

Figure 45: Daily peak flows comparison between 2019-2020 and 2094-2095 at Högsmölla

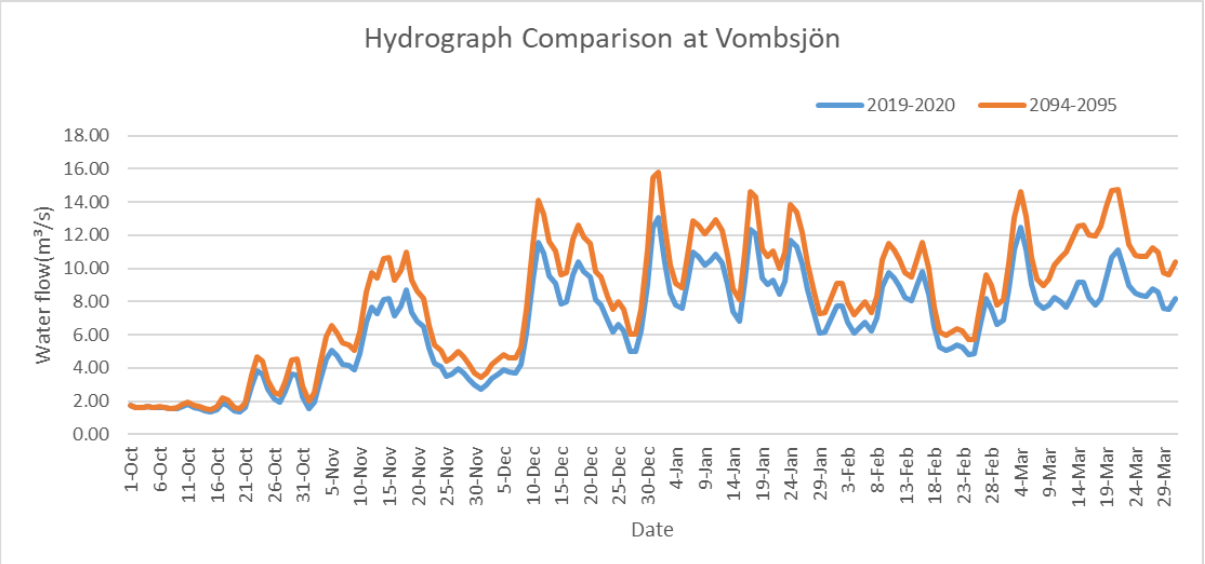

Figure 46: Daily peak flows comparison between 2019-2020 and 2094-2095 at Vombsjön

6. Discussion and Limitations

All models are simplifications of the real world (Moradkhani and Sorooshian, 2008). There is always going to be room for improvement. The inaccuracy of the simulated flow compared with the observed flow can be described for many reasons, such as data availability, methods simplification, and so on. Further, the climatic conditions, geological factors, and topographical factors have a great impact on accuracy.

- Curve numbers are used for reflecting the soil moisture condition and the antecedent moisture condition, which are combined by using empirical formulas. Then, only a single soil moisture value is provided although the curve numbers can be adjusted within a range during calibration. While soil moisture shows considerable spatial heterogeneity and varies with time, consequently, which may not reflect the above-described variance in space and time. Also, average Curve numbers for each sub-basin are used to describe rainfall-runoff processes, which may also reduce the accuracy. If the magnitude of variation increases, the accuracy decreases.

- The imperviousness area calculation only includes the urban area and roads. As well as this, the land cover is changing such as urbanization or reducing bare land. Further, whether the impervious area outlet is directly connected to the drainage system is not considered.

- Historical discharge data are an important source of information and have a great impact on flood return frequency. In this study, only 45 years of data were used for flood frequency analysis. Also, other factors such as climate change, or land-use variation changes may impact flood runoff. So the flood series tends to exhibit non-stationarity, and a certain magnitude of the return period may change as well (Machado *et al.*, 2015).

- Daily precipitation from eight stations from 1996 to 2020 was collected. Due to the arbitrary nature of the climate, there is a possibility of providing different results by using other observation data which brings uncertainties. Further, the precipitation data at Lund is used for the precipitation frequency analysis since it has a long time series. Although there is a good correlation between the cumulative annual precipitation at Lund and the cumulative annual precipitation at adjacent stations, there are still some uncertainties since the peak values are evened out by using the double mass curve method.

- HEC-HMS model could be used to determine and predict significant flood peaks and threshold runoff values when the discrepancy between the simulated and observed values is small. Also, the cumulative threshold precipitation that can trigger floods can also be determined (Czigány, Pirkhoffer and Geresdi, 2010).

- The hypothetical storm method is used for the event-based flood analysis. It assumes that all subbasins receive the same amount of precipitation while in reality that would be not the case. Also, this method works well for small catchments. In this study, the drainage area is about 1150 km^2. As a result, the accuracy may decrease.

- The assessment of the impacts of climate change on the hydrological model is based on the current condition. The variation of land use and imperviousness area etc in the future are not considered.

- The non-linear relationship between the precipitation and runoff generation was investigated before, while the flood forecast by ensemble methods is becoming increasingly important for operational purposes.

7. Conclusion

The hydrological model in HEC-HMS is a widely used method for river catchment management, simulation of continuous and event-based watershed responses and generation of flood hydrographs. The rainfall-runoff simulation results can be useful for well-planned programmes in resource management projects and water conservation, and the results with climate change can be used for future prediction of runoff for flood mitigation strategies in the catchment.

The simulated flow of the continuous calibration match well with the observed flow. The volume errors vary between 1.7% and 22% and the magnitude discrepancies vary from 1.7% to 35%, only the value in 2004-2005 is a little out of range (±30%). The reason is that the model is calibrated in many different years, and a compromise has to be made between each other. For the peak flow, overall, the computed peak flow is less than the observed flow, specifically in 2007-2008 (the wet years). The average peak error during the wet year increases by 4.2% compared with the average value in the normal and dry years. It may be caused by the relatively low Curve number that underestimates actual moisture conditions during the wet year. Also, it impacts the event-based simulation since all parameters are identical to the continuous simulation.

The hydrologic model with RCP8.5 climate change is used to evaluate the effects of climate change on flood events. Climate change will continue to put pressure on societies. For the continuous simulation, the increase in precipitation and temperature led to around a 24% increase in peak flow at the outlet. For the event-based simulation, the precipitation for 2-year, 5-year, 10-year, 25-year, 50-year, and 100-year events are simulated, and the overall increase of peak flow is about 20%. While the simulated peak flow with climate change is around 8% less than the published average peak flow with RCP 8.5 from SMHI.

Finally, based on the evaluation criteria statistics, it can be concluded that the Rainfall-runoff analysis computed flow is highly correlated with the observed in most cases although there are still some uncertainties. As mentioned in the discussion part, the non-linear relationship between the precipitation and runoff generation was investigated by some researchers. Consequently, the ensemble methods for flood forecast are becoming increasingly dominant and it reduces the potential forecast errors for operational purposes (Komma et al., 2007). A further study needs to be done in the future.

8. References

Bahramian, K., Nathan, R., Western, A. W. & Ryu, D. (2021). Towards an Ensemble-Based Short-Term Flood Forecasting Using an Event-Based Flood Model- Incorporating Catchment-Average Estimates of Soil Moisture, *Journal of Hydrology*, vol. 593, p.125828.

Beard, L. R. (1962). Statistical Methods in Hydrology, Army Engineer District, Sacramento.

Chifflard, P., Kranl, J., Strassen, G. zur & Zepp, H. (2018). The Significance of Soil Moisture in Forecasting Characteristics of Flood Events. A Statistical Analysis in Two Nested Catchments, *Journal of Hydrology and Hydromechanics*, vol. 66, no. 1, pp.1–11.

Cronshey, R. G., Roberts, R. T. & Miller, N. (1985). Urban Hydrology for Small Watersheds (TR-55 Rev.), Hydraulics and Hydrology in the Small Computer Age, 1985, ASCE, pp.1268–1273, Available Online: https://cedb.asce.org/CEDBsearch/record.jsp?dockey=0045976 [Accessed 23 May 2022].

Czigány, S., Pirkhoffer, E. & Geresdi, I. (2010). Impact of Extreme Rainfall and Soil Moisture on Flash Flood Generation, p.23.

England Jr., J. F., Cohn, T. A., Faber, B. A., Stedinger, J. R., Thomas Jr., W. O., Veilleux, A. G., Kiang, J. E. & Mason, Jr., R. R. (2019). Guidelines for Determining Flood Flow Frequency — Bulletin 17C, USGS Numbered Series, 4-B5, *Guidelines for Determining Flood Flow Frequency — Bulletin 17C*, Vol. 4-B5, Reston, VA: U.S. Geological Survey, p.168, Available Online: http://pubs.er.usgs.gov/publication/tm4B5 [Accessed 23 May 2022].

ERSI, Sentinel-2 10m Land Use/Land Cover Timeseries - Overview. (2022). , Available Online: https://www.arcgis.com/home/item.html?id=d3da5dd386d140cf93fc9ecbf8da5e31 [Accessed 22 May 2022].

Eslamian, S. (2014). Handbook of Engineering Hydrology: Environmental Hydrology and Water Management, CRC Press.

Hall, M., Lund, E., Rummukainen, M., Lunds universitet, & Centrum för miljö- och klimatforskning. (2015). Klimatsäkrat Skåne, Lund: Centrum för miljö- och klimatforskning, Lunds universitet.

Komma, J., Reszler, C., Blöschl, G. & Haiden, T. (2007). Ensemble Prediction of Floods – Catchment Non-Linearity and Forecast Probabilities, *Natural Hazards and Earth System Sciences*, vol. 7, no. 4, pp.431–444.

Lantmäteriet – vi Känner till Varenda Plats i Sverige. (2022). *Lantmateriet.Se*, Available Online: https://www.lantmateriet.se/ [Accessed 22 May 2022].

Machado, M. J., Botero, B. A., López, J., Francés, F., Díez-Herrero, A. & Benito, G. (2015). Flood Frequency Analysis of Historical Flood Data under Stationary and Non-Stationary Modelling, *Hydrology and Earth System Sciences*, vol. 19, no. 6, pp.2561–2576.

Maskey, S. & ProQuest (Firm). (2004). Modelling Uncertainty in Flood Forecasting Systems Dissertation, Netherlands: A.A. Balkema.

Moradkhani, H. & Sorooshian, S. (2008). General Review of Rainfall-Runoff Modeling: Model Calibration, Data Assimilation, and Uncertainty Analysis, in S. Sorooshian, K.-L. Hsu, E. Coppola, B. Tomassetti, M. Verdecchia, & G. Visconti (eds), *Hydrological Modelling and the Water Cycle: Coupling the Atmospheric and Hydrological Models*, [e-book] Berlin, Heidelberg: Springer, pp.1–24, Available Online: https://doi.org/10.1007/978-3-540-77843-1_1 [Accessed 23 May 2022].

Ross, C. W., Prihodko, L., Anchang, J., Kumar, S., Ji, W. & Hanan, N. P. (2018). Global Hydrologic Soil Groups (HYSOGs250m) for Curve Number-Based Runoff Modeling, p.571.82448 MB.

Scharffenberg, W. A. (2013). HEC-HMS User's Manual, p.442.

SMHI, In-Depth Climate Scenario Service. (2022a). , Available Online: https://www.smhi.se/klimat/framtidens-klimat/fordjupade-klimatscenarier/met/sverige/medelnederbord/rcp85/2071-2100/year/anom [Accessed 22 May 2022].

SMHI, In-Depth Climate Scenario Service. (2022b). , Available Online: https://www.smhi.se/klimat/framtidens-klimat/fordjupade-klimatscenarier/hyd/kavlingean/maximalvattenforing50/rcp85/2071-2100/year [Accessed 24 May 2022].

USDA, Urban Hydrology for Small Watersheds. (1986). , Available Online: https://www.nrcs.usda.gov/Internet/FSE_DOCUMENTS/stelprdb1044171.pdf [Accessed 22 May 2022].

Vattenrådet – Kävlingeån. (2022). , Available Online: http://www.xn--kvlingen-0zaq.se/vattenradet/ [Accessed 22 May 2022].

Appendix A

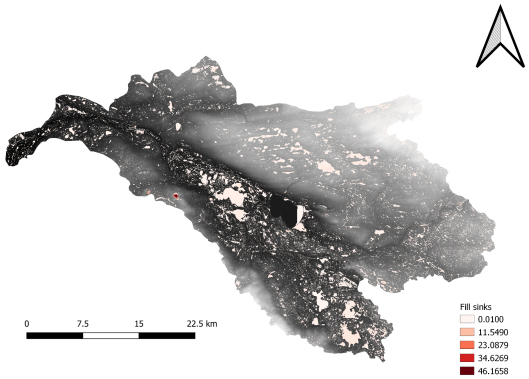

A.1: Filled sinks of Kävlinge River Basin

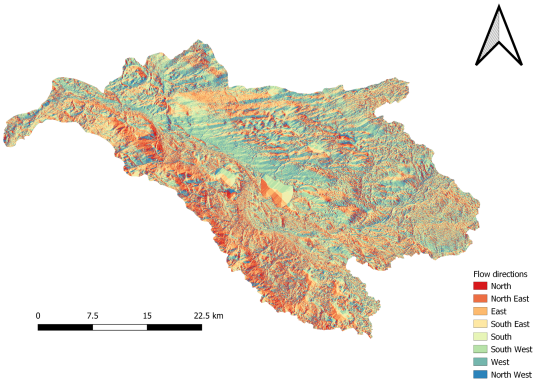

A.2: Flow directions in Kävlinge River Basin

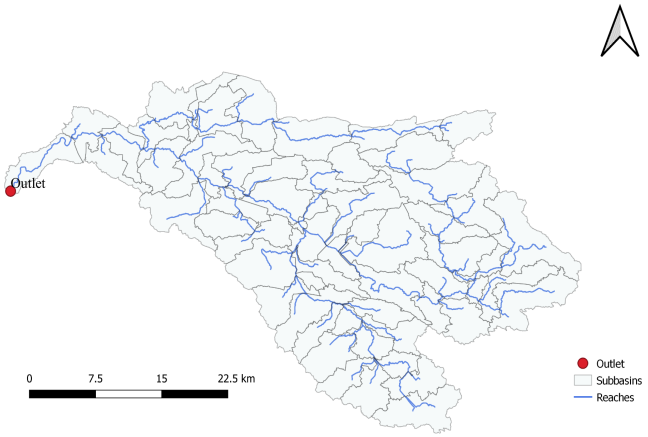

A.3: Modelled subbasins and streams in Kävlinge River Basin

Appendix B

B.1: Probability and return period for annual daily maximum precipitation in Lund for 1900-2020. Only the 10 highest and 10 lowest values are presented.

Rank	Daily max (mm)	Year	Probility	Return period
1	81.2	1941	0.8%	119.00
2	70.6	1914	1.7%	59.50
3	61.8	1930	2.5%	39.67
4	59.7	1931	3.4%	29.75
5	58.2	2007	4.2%	23.80
6	57.5	2016	5.0%	19.83
7	56.3	1963	5.9%	17.00
8	54.3	1981	6.7%	14.88
9	53.8	1920	7.6%	13.22
10	53	1901	8.4%	11.90
109	21.2	1966	91.6%	1.09
110	20.4	2004	92.4%	1.08
111	20	1973	93.3%	1.07
112	19.7	1924	94.1%	1.06
113	19.6	1971	95.0%	1.05
114	19.4	1926	95.8%	1.04
115	17.4	1991	96.6%	1.03
116	16.6	1953	97.5%	1.03
117	16.3	1944	98.3%	1.02
118	12.1	1957	99.2%	1.01

Appendix C

C.1: The correlation plot of simulated versus observed flow at different calibration stations from 2014-2015

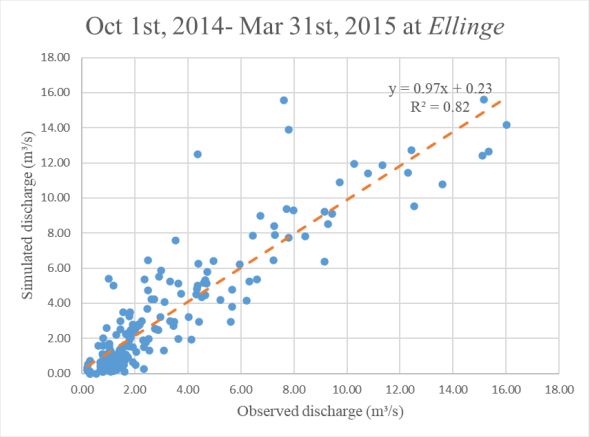

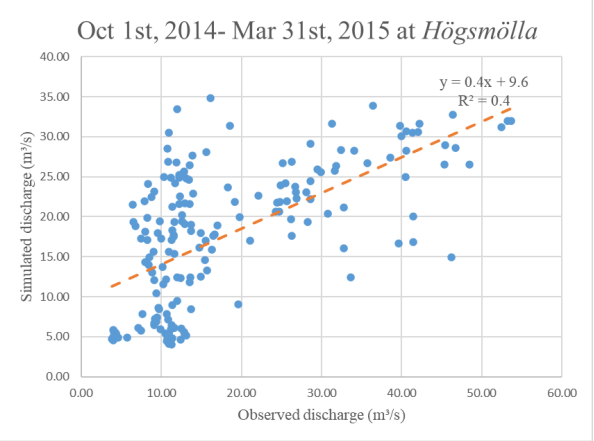

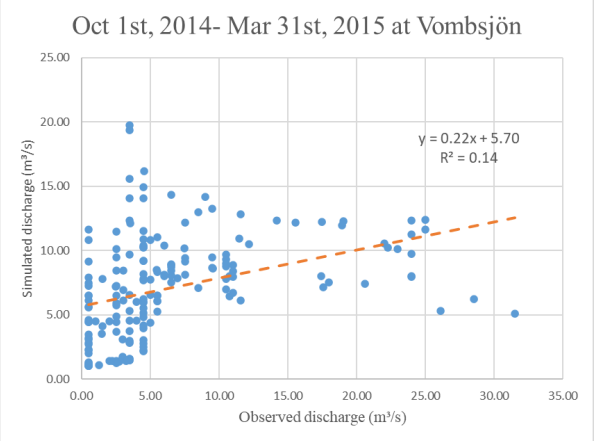

C.2: The correlation plot of simulated versus observed flow at different calibration stations from 2018-2019

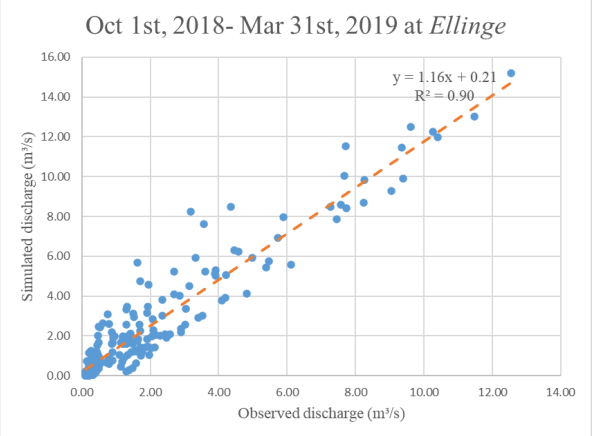

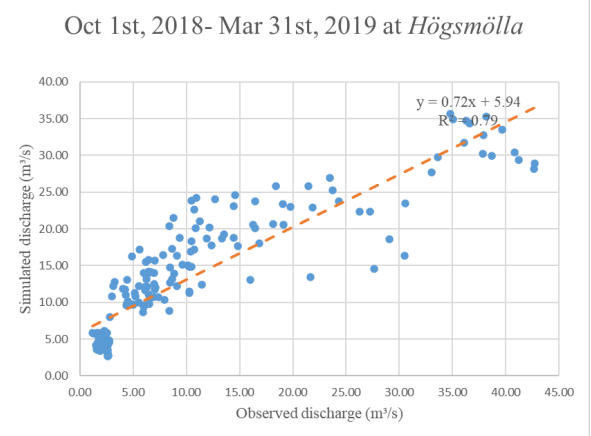

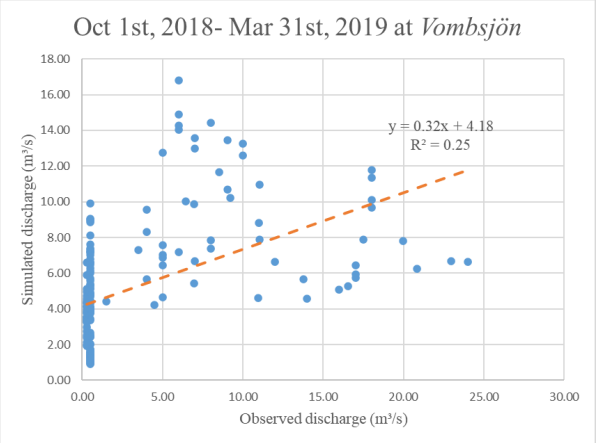

C.3: The correlation plot of simulated versus observed flow at different calibration stations from 2019-2020

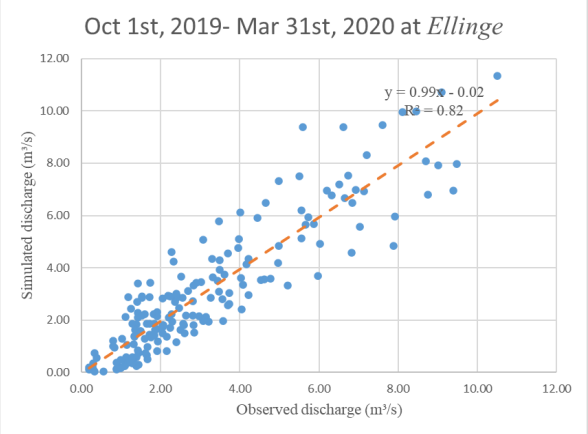

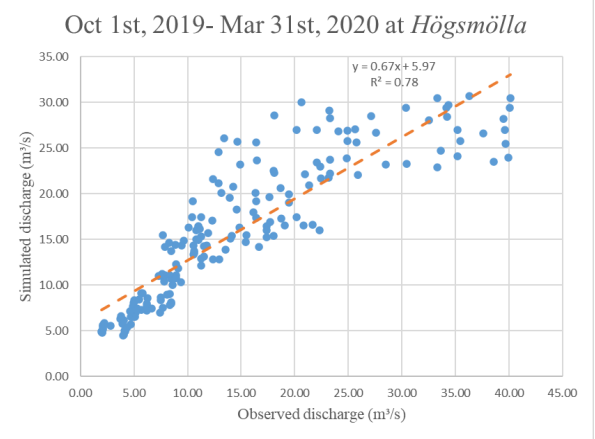

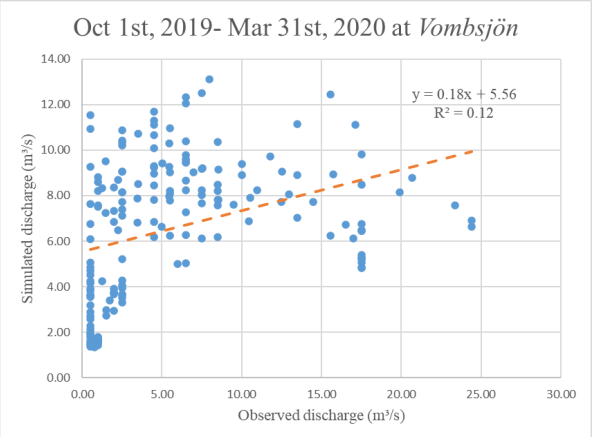

C.4: The correlation plot of simulated versus observed flow at different calibration stations from 2007-2008